Scientific Research Publishing

Open Journal of Geology, 2026, 16(2), 104-137
https://www.scirp.org/journal/ojg
ISSN Online: 2161-7589
ISSN Print: 2161-7570

Petrology of Gneisses and the Associated Granites from Devanahalli Area, Karnataka, Southern India

Priyanka Harohalli Subramani, Shadaksharaswamy Nagabhushan

Department of Geology, Bangalore University, Bangalore, India
Email: priyankahsubramani@gmail.com, nsswamy@rediffmail.com

How to cite this paper: Harohalli Subramani, P. and Nagabhushan, S. (2026) Petrology of Gneisses and the Associated Granites from Devanahalli Area, Karnataka, Southern India. *Open Journal of Geology*, **16**, 104-137.
https://doi.org/10.4236/ojg.2026.162007

Received: January 5, 2026
Accepted: February 25, 2026
Published: February 28, 2026

Abstract

Granites and gneisses are the principal lithological components of the Precambrian crystalline terrain in Devanahalli Taluk, Bangalore Rural District, southern India, within the eastern segment of the Dharwar Craton. This study synthesizes field observations, petrographic analysis, and whole-rock geochemical data to delineate the characteristics, genesis, and tectonic relevance of these rocks. Field investigations reveal that the gneisses typically manifest as well-banded to streaky units exhibiting pronounced foliation, and are locally intruded by younger granitic bodies, pegmatites, and quartz veins. Petrographic examination identifies mineral assemblages primarily composed of quartz, plagioclase, K-feldspar, biotite, and hornblende, accompanied by accessory phases such as zircon, apatite, and opaque minerals. Major element geochemistry indicates that the granites are silica-enriched and range from peraluminous to weakly metaluminous, while the gneisses show tonalitic to granodioritic compositions. Trace and rare earth elements (REEs) highlight REE enrichment and negative Eu anomalies, consistent with plagioclase fractionation and crustal involvement. Integrated petrographic and geochemical evidence suggests that these granites and gneisses resulted from Archaean crustal evolution processes, including partial melting of older TTG-type crust followed by deformation and metamorphism. The record preserved in these rocks is indicative of significant crust-forming events associated with the stabilization of the Dharwar Craton.

Keywords

Granite, Gneiss, Petrology, Dharwar Craton, Devanahalli, Southern India

1. Introduction

Granites and gneisses represent the principal constituents of Archaean continental crust and preserve crucial evidence for early crust-forming processes, magma genesis, and tectono-metamorphic evolution. Tonalite-trondhjemite-granodiorite (TTG) suites, which dominate many Archaean terrains worldwide, are widely interpreted as products of partial melting of hydrated basaltic crust under high-pressure conditions [1]-[3]. Subsequent crustal reworking through deformation, metamorphism, and partial melting resulted in the generation of diverse granitoid compositions during craton stabilization [4] [5]. The Dharwar Craton of southern India is one of the oldest and best-exposed Archaean cratonic blocks and is characterized by extensive exposures of granites and gneisses belonging to the Peninsular Gneissic Complex (PGC) [6] [7]. Previous studies have documented multiple phases of magmatism, deformation, and metamorphism within the craton, reflecting prolonged crustal growth from Paleoarchean to Neoarchean convergence [1] [6] [8]. However, detailed integrated petrographic and geochemical studies of granites and gneisses from specific localities such as Devanahalli remain limited. The present study addresses this gap by providing a comprehensive field-based, petrographic, and geochemical evaluation of granites and gneisses from the Devanahalli area, Karnataka.

2. Geological Setting

The study area (**Figure 1**) is situated in the eastern part of the Dharwar Craton and is dominantly underlain by Archaean rocks of the Peninsular Gneissic Complex [6] [7]. The PGC comprises compositionally banded tonalitic, trondhjemitic, granodioritic, and granitic gneisses intruded by younger granites, pegmatites, and quartz veins [8]. These lithologies represent multiple phases of crustal growth, reworking, and stabilization from Paleo- to Neoarchean times [1] [9].

Structurally, the gneisses exhibit well-developed gneissic banding and regional foliation defined by alternating felsic and mafic mineral layers. The dominant foliation trends NW-SE to NNW-SSE and are locally affected by microfolding, boudinage, and shear zones, indicating polyphase deformation. Metamorphic assemblages suggest amphibolite- to granulite-facies conditions [10], consistent with deep crustal reworking during craton stabilization and prolonged tectonic evolution [11].

3. Materials and Methods

Representative granite and gneiss samples were systematically collected from fresh, unweathered outcrops across the Devanahalli area, Karnataka, covering the major lithological varieties identified during field mapping. A total of twenty-five samples, comprising sixteen granites and nine gneisses, was selected for detailed petrographic and geochemical investigations.

Hand specimens were cleaned, trimmed, and processed for thin section preparation. Standard petrographic thin sections of approximately 30 μm thickness

were prepared and examined under a polarizing microscope to document mineralogy, textures, and microstructures.

For geochemical analysis (**Tables 1-8**), selected samples were crushed using a steel jaw crusher and powdered in an agate mill to avoid contamination. Major element oxides were analyzed using X-ray fluorescence spectrometry (XRF), whereas trace and rare earth elements were determined using Inductively Coupled Plasma-Optical Emission Spectrometry (ICP-OES) and Inductively Coupled Plasma-Mass Spectrometry (ICP-MS) techniques, respectively. Analytical precision for major oxides is better than ±1% - 2%, and for trace and rare earth elements, better than ±5%.

Calibration and quality control were ensured through repeated analyses of international reference rock standards and procedural blanks. The geochemical data obtained were further processed to construct variation diagrams, discrimination plots, and chondrite-normalized rare earth element patterns using standard normalization values after Taylor and McLennan (1985).

4. Field Characteristics

Field observations indicate that gneisses are medium- to coarse-grained and display prominent compositional banding, streaky foliation, and augen structures. These features are characteristic of high-grade metamorphic terrains subjected to intense ductile deformation. Mafic-rich layers dominated by biotite and hornblende alternate with felsic quartz-feldspar-rich bands, reflecting original compositional heterogeneities and subsequent metamorphic differentiation [12].

Foliated/Streaky gneisses are well exposed near Avathi and Chikkobanahalli in the northern part of the study area. The streaky variety of biotite gneiss is dioritic to granodioritic in composition. The light-colored bands are quartz-rich and granoblastic, while the darker layers are rich in biotite and display schistosity at finer scales (**Figure 2(a)**, **Figure 2(b)**). The banded gneisses are best exposed around the Chikkagollahalli and Hurulugurki area and exhibit clear banding, wherein quartzofeldspathic minerals and mafic minerals occur as alternate bands. The banded gneiss (**Figure 3(a)**) is of the granodiorite type. Migmatitic gneisses are granodioritic in composition and show characteristic migmatitic structures as illustrated by Mehnert [12], viz., schollen, stromatic, phlebitic, ptygmatic, etc., and these structures are best exposed in a quarry south of Tubugere and Hurulagurki areas. In some portions, these are converted into banded gneisses. Migmatitic gneisses (**Figure 3(b)**) in the study area are prominently exposed as rugged, weather-resistant outcrops with characteristic swirled or irregular banding, reflecting partial melting and melt segregation processes that these rocks have undergone.

Granitic bodies occur as massive to weakly foliated intrusions cross-cutting the gneissic fabric, suggesting their emplacement after the main deformation events affecting the host gneisses. Xenoliths of gneiss within granite bodies indicate assimilation of older crustal material during magma ascent and emplacement. Peg-

matite and quartz veins are widespread and are either concordant or discordant to foliation, representing late-stage magmatic and hydrothermal activity.

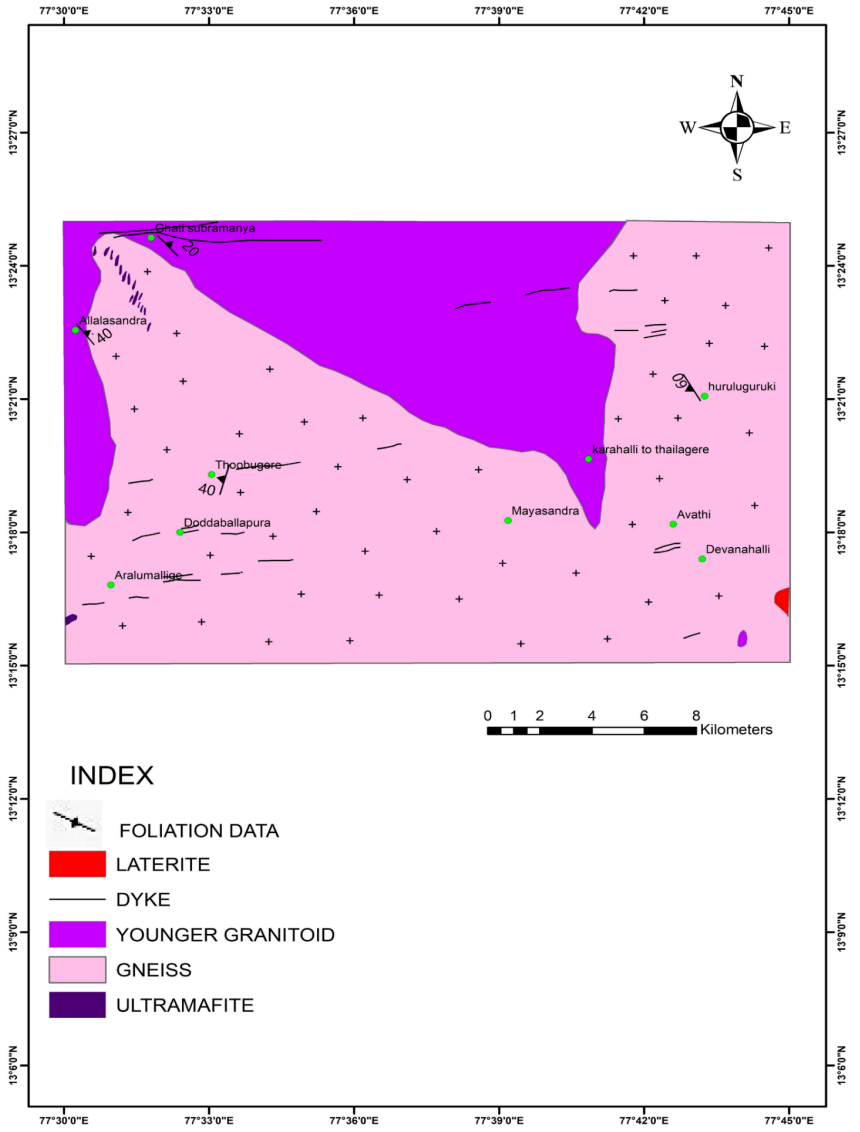

Figure 1. Geological map of the study area.

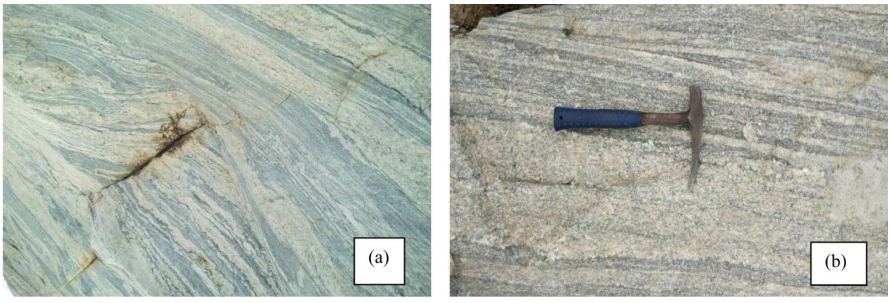

Figure 2. Field photograph of gneiss. (a) Foliated gneiss with some fractures. (b) Quartzofeldspathic gneiss exhibiting very well-developed foliation with alternating bands of light and dark-colored layers.

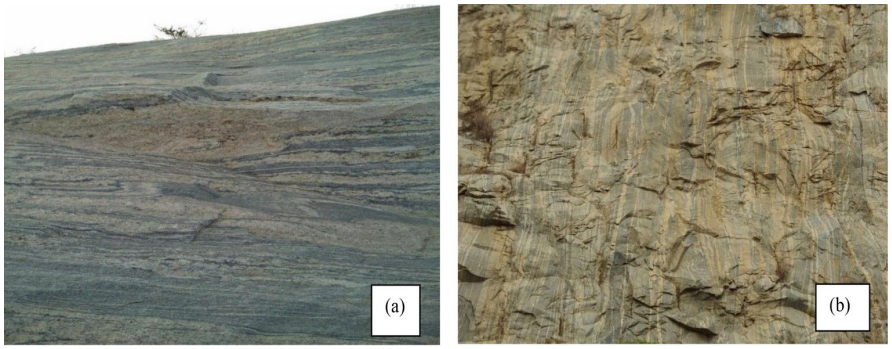

Figure 3. Field photograph of gneiss. (a) Stretched banded gneiss with the presence of asymmetric augens. (b) Banded migmatitic gneisses with well-developed alternating dark and light-colored bands.

Grey medium-grained granite variety is best exposed around Dasarahalli, Chikkagollahalli, and Chikkobanahalli areas. These are massive, greyish-white colored leucocratic rocks. The rock is traversed by innumerable epidote veins. The rock is highly jointed, fine-grained, grey, and cut by epidote veins (Figure 4(a)).

Medium-grained pink granite (Figure 4(b)) is best seen in the areas of Thailagere, Hurulugurki, and Chikkagollahalli. This granite is intrusive into the grey medium granite. It is a massive, pinkish-red colored, leucocratic rock. The felsic minerals include K-feldspar and quartz; the mafic minerals include biotite and hornblende. The exposed outcrop represents a medium-grained rock, characterized by a uniform, equigranular texture and a massive appearance with little foliation.

Numerous veins of pegmatites and quartz veins are seen distributed all over the study area. The vein quartz (Figure 5(a)) is milky white in color and barren of mineralization. Pink pegmatite veins (Figure 5(b)) of varying width ranging from 5 cm to 0.5 m traverse the foliation planes of gneisses. Pegmatite and quartz veins (Figure 6) are typically late- to post-tectonic intrusions, and their geometry helps to interpret deformation timing. Pegmatites are often intruded along foliation planes, while quartz veins may follow late brittle structures or pressure-solution seams.

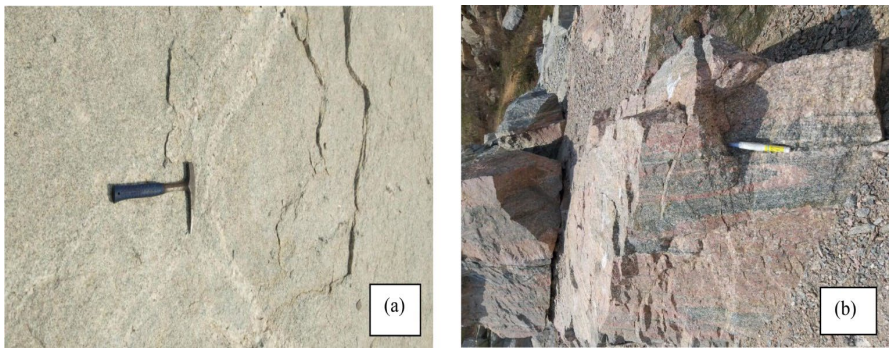

Figure 4. (a) Field photograph of fine-grained grey granite. (b) Pink granite with a gneiss enclave which shows alternate pink and dark bands within gneisses.

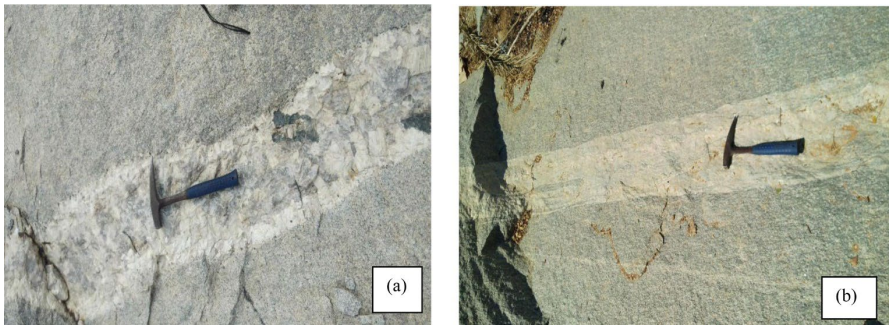

Figure 5. (a) Field photograph of barren vein quartz shows milky white color with some biotite in the host of schlieren's. (b) Pink pegmatite vein intrusion along the foliation planes of gneisses.

Figure 6. Field photograph of a quartz vein intruded into the fracture zone of a highly weathered granitic rock.

5. Petrography

Gneisses are composed mainly of quartz, plagioclase, K-feldspar, biotite, and hornblende, with accessory zircon, apatite, and opaque minerals. It usually shows granoblastic texture and myrmekitic textures (**Figure 7(a)**). Quartz commonly exhibits undulose extinction and recrystallized grain boundaries, showing marginal granulation (**Figure 7(b)**), indicating deformation under high-temperature conditions [10] [12]. Plagioclase shows polysynthetic twinning and partial sericitization (**Figure 8(a)**), K-feldspar occurs as microcline with cross-hatched twinning, and perthitic intergrowth (**Figure 8(b)**). Biotite and hornblende occur as aligned flakes defining the gneissic foliation **Figure 9(a)**, **Figure 9(b)**. **Figure 10(a)**, **Figure 10(b)** shows that biotite grains frequently contain epidote and sphene, as well as some iron oxides. Biotites are altered into chlorite [13], showing crenulation cleavage (**Figure 11(a)**). Sphene, when present, occurs as spongy wedge-shaped grains in mafic-rich layers (**Figure 11(b)**. Magmatic epidote is observed (**Figure 12(a)**), some magmatic epidotes are associated with biotite and hornblende (**Figure 12(b)**) and some are associated with allanite in the core (**Figure 13**).

The observed mineral assemblages and microstructures are consistent with amphibolite- to granulite-facies metamorphism and prolonged ductile deformation,

typical of Archaean gneissic terrains.

Granites display coarse-grained, hypidiomorphic granular textures (**Figure 14(a)**, **Figure 14(b)**), typical of plutonic rocks. Quartz occurs as anhedral interstitial grains, while K-feldspar is represented by microcline and orthoclase, commonly exhibiting perthitic textures (**Figure 15(a)**) and myrmekitic texture (**Figure 15(b)**). Plagioclase is subhedral and locally altered to sericite (**Figure 16(a)**). Biotite is the dominant mafic mineral, with minor hornblende in some samples. Biotite (5-8%) is brown to dark brown in color, pleochroic, showing perfect cleavage and exhibits partial alteration to chlorite associated with monazite (**Figure 16(b)**). Marginal granulation is a common feature (**Figure 17(a)**). Grain size reduction, elongation, and mylonitic fabric development of grains (**Figure 17(b)**) are often seen due to shearing, composed of quartz, plagioclase, biotite, and K-feldspar. Magmatic epidote is associated with quartz-plagioclase-K-feldspar and chloritized biotite (**Figure 18(a)**, **Figure 18(b)**). Magmatic epidote-sphene-chlorite association is also observed (**Figure 19(a)**). Shear planes with S-C plane development and grain size reduction are also observed (**Figure 19(b)**). Hydrothermal activity in fracture fillings is seen in **Figure 20(a)** & **Figure 20(b)**. Isotropic fluorite is observed (**Figure 21(a)**), and chlorite shows Berlin blue color (**Figure 21(b)**). Some zoned zircon is seen associated with muscovite and chlorite (**Figure 22(a)**, **Figure 22(b)**).

The mineralogical characteristics are consistent with crust-derived granitic magmas formed through partial melting processes [4] [5].

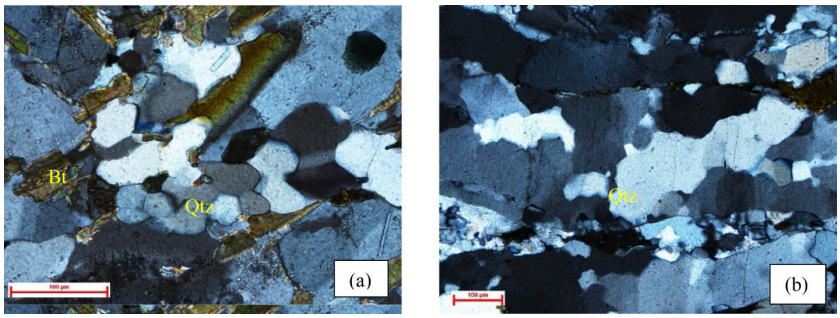

Figure 7. Microphotograph of gneiss. (a) Granoblastic texture composed of Qtz + Bt under crossed nicols. (b) Marginal granulation of quartz under crossed nicols.

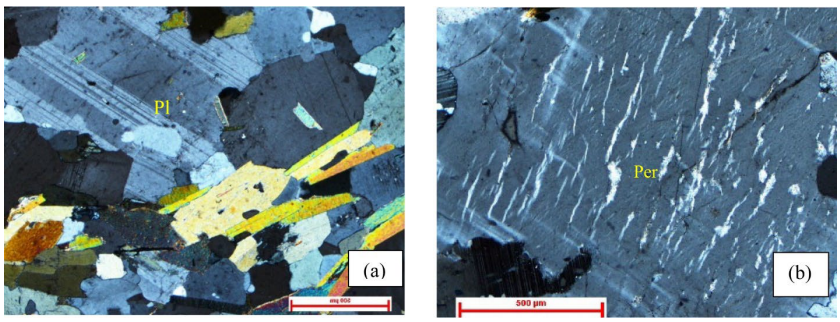

Figure 8. Microphotograph of gneiss. (a) Plagioclase shows polysynthetic twinning under crossed nicols. (b) Perthitic texture under crossed nicols.

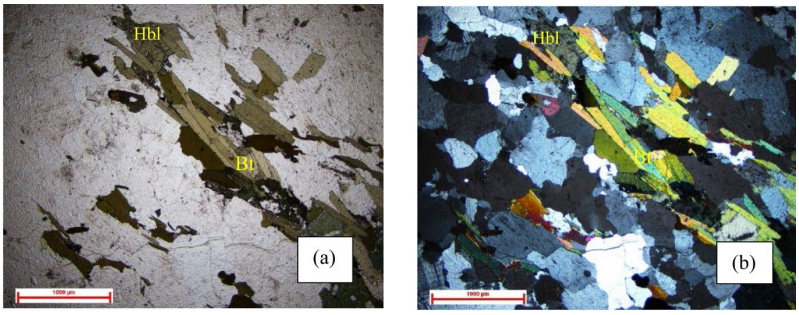

Figure 9. Microphotograph of gneiss. (a) Foliation defined by the alignment of biotite and hornblende under plane-polarised light. (b) Foliation defined by the alignment of biotite and hornblende under crossed nicols.

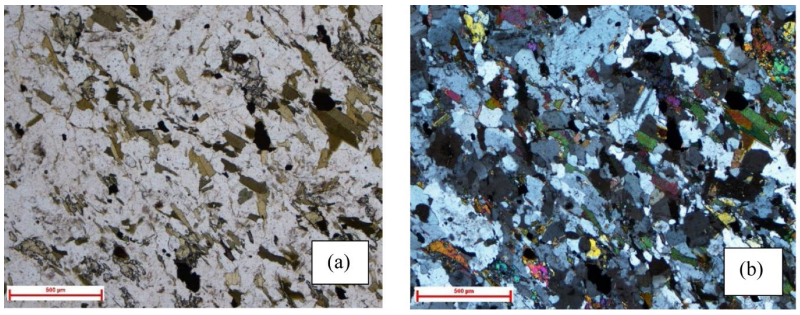

Figure 10. Microphotograph of gneiss. (a) Foliation defined by biotite alignment associated with epidote-sphene-iron oxide under plane polarized light. (b) Foliation defined by biotite alignment associated with epidote-sphene-iron oxide under crossed nicols.

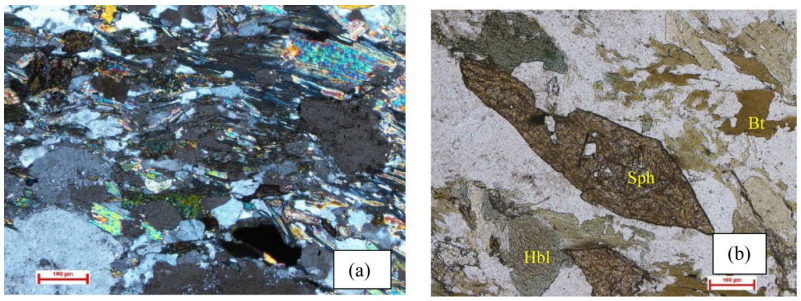

Figure 11. Microphotograph of gneiss. (a) Crenulation cleavage development and chloritization of biotite in biotite-hornblende under crossed nicols. (b) Sphene-hornblende-biotite association in biotite-hornblende under plane polarized light.

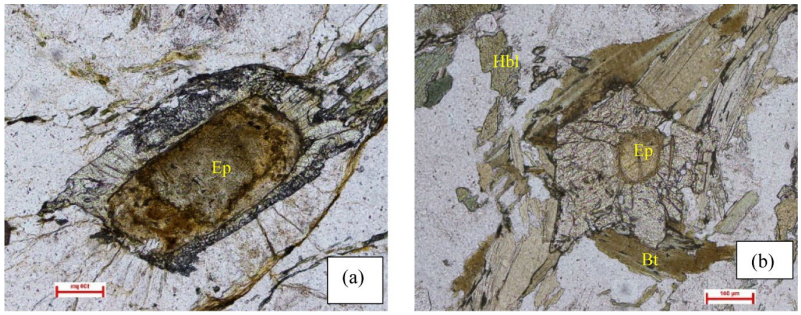

Figure 12. Microphotograph of gneiss. (a) Magmatic epidote under plane-polarized light. (b) Magmatic epidotes associated with biotite-hornblende under plane-polarized light.

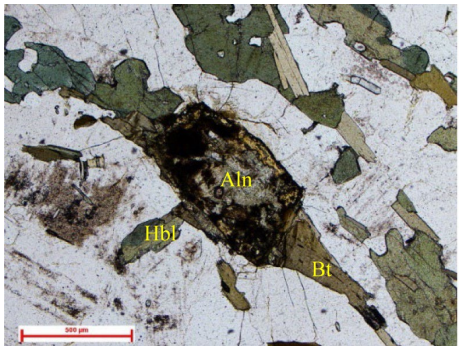

Figure 13. Microphotograph of allanite in association with biotite and hornblende in quartzo-feldspathic gneiss, defining the foliation under plane polarized light.

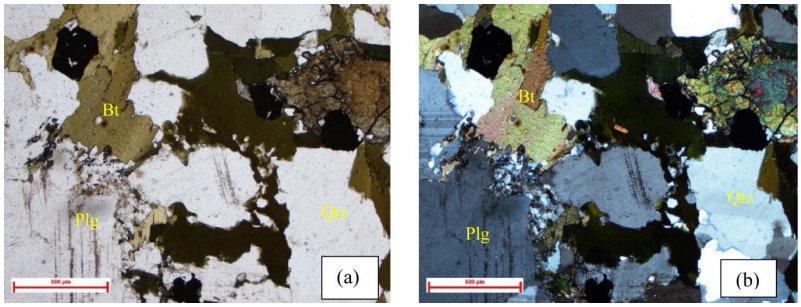

Figure 14. Microphotograph of granite. (a) Hypidiomorphic texture composed of Qtz-Plg-Bt under plane-polarised light. (b) Hypidiomorphic texture composed of Qtz-Plg-Bt under crossed nicols.

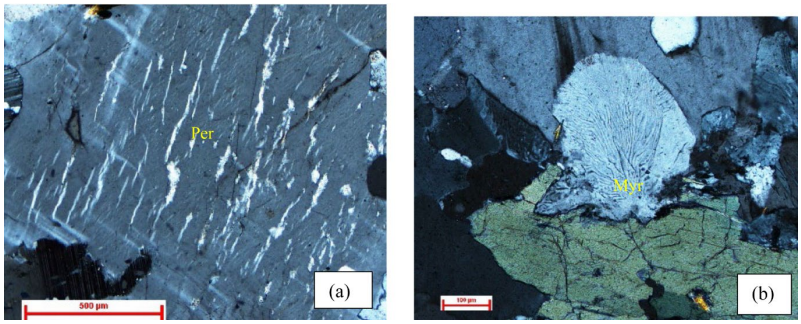

Figure 15. (a) Perthitic texture in grey porphyritic granite under crossed nicols. (b) Myrmekitic texture in grey porphyritic granite under crossed nicols.

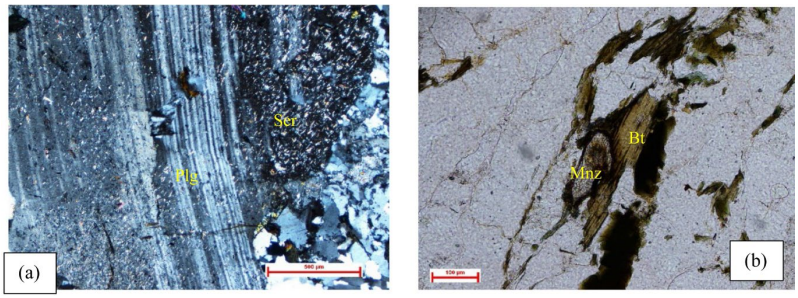

Figure 16. Microphotograph of granite. (a) Plagioclase showing bending of twin lamellae and sericitization under crossed nicols. (b) Monazite-biotite association under plane polarized light.

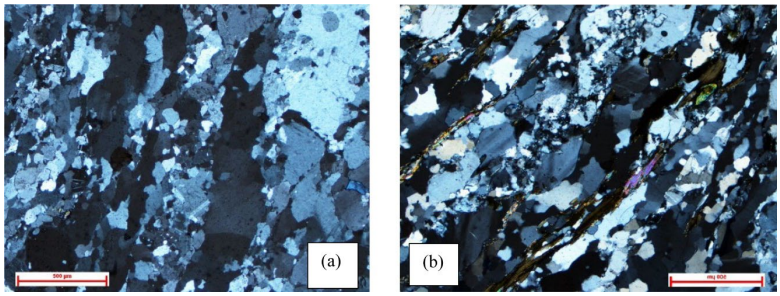

Figure 17. Microphotograph of granite. (a) Marginal granulation and strain shadow effect in quartz under crossed nicols. (b) Grain size reduction, elongation, and mylonitic fabric development of grains composed of quartz, plagioclase, biotite, and k-feldspar under crossed nicols.

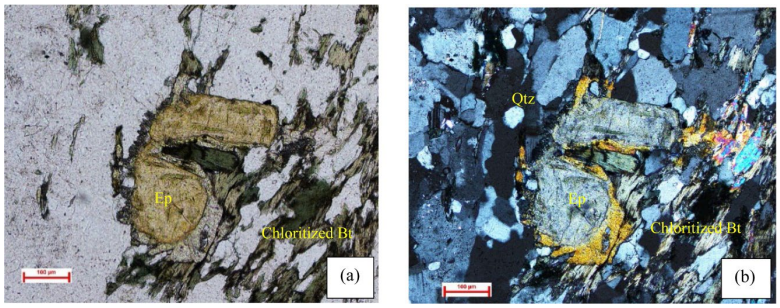

Figure 18. Microphotograph of granite. (a) Magmatic epidote in association with quartz-plagioclase-K-feldspar and chloritized biotite under plane-polarised light. (b) Magmatic epidote in association with quartz-plagioclase-K-feldspar and chloritized biotite under crossed nicols.

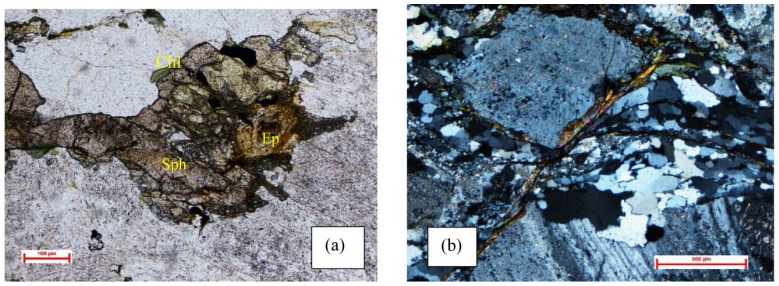

Figure 19. Microphotograph of granite. (a) Magmatic epidote-sphene-chlorite association under plane-polarised light. (b) Shear planes with S-C plane development and grain size reduction under crossed nicols.

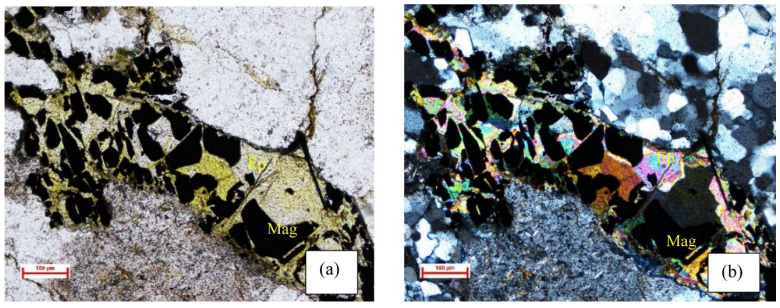

Figure 20. Microphotograph of granite. (a) Fracture-filling magnetite and epidote under plane polarized light. (b) Fracture-filling magnetite and epidote under crossed nicols.

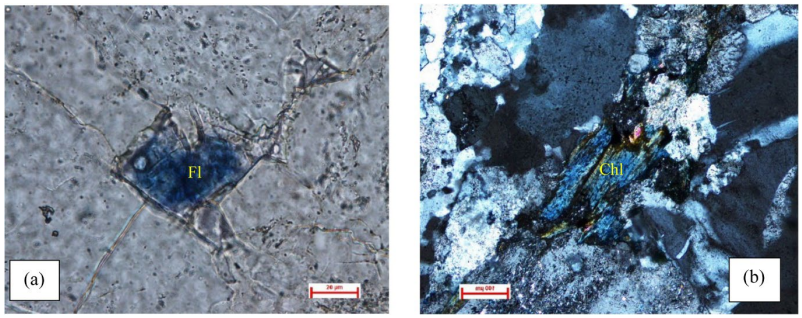

Figure 21. Microphotograph of granite. (a) Fluorite under plane-polarised light. (b) Chlorite showing Berlin blue colour under crossed nicols.

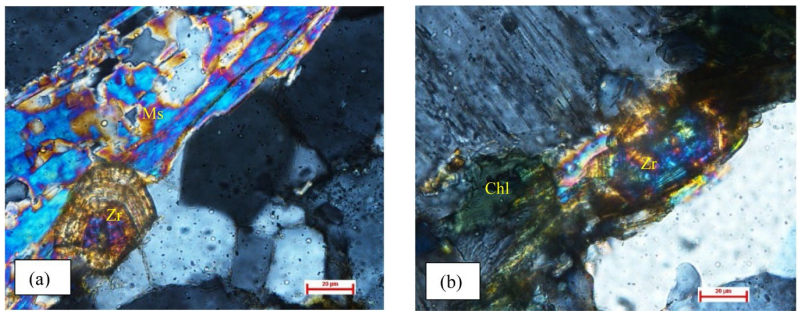

Figure 22. Microphotograph of granite. (a) Zoned zircon in association with muscovite under crossed nicols. (b) Zoned zircon associated with chlorite under crossed nicols.

6. Geochemistry

The major, trace, and rare earth elemental compositions and CIPW calculations of gneisses are listed in Tables 1-4.

The major elements of gneisses show a considerable range in composition, with SiO_2 ranging from 75.17 to 63.49% with an average of 72.24%, Al_2O_3 from 13.28 to 14.53% with an average of 14.35%, TiO_2 from 0.08 to 0.86% with an average of 0.21%, Fe_2O_3 from 0.63 to 1.89% with an average of 1.25%, and MgO from 0.05 to 0.42% with an average of 0.25%. Higher Fe_2O_3 and MgO in two samples are mainly due to the presence of hornblende and biotite in appreciable amounts in mineralogy. CaO ranges from 0.73 to 3.01% with an average of 1.50%, and Na_2O from 3.62 to 5.92% with an average of 4.43%. In addition to this, one sample shows higher CaO (4.43%). K_2O ranges from 0.41 to 5.26% with an average of 3.07%. The K_2O/Na_2O ratio in gneisses ranges from 0.39 to 1.35. Gneisses of the study area are characterized by low to moderate content of ferromagnesian elements (Fe_2O_3 + MgO + TiO_2 = 1.0 to < 10%). In the study area, three samples (7, 8, and 9) show higher Na2O relative to CaO and K_2O.

In Harker's variation diagram (Figure 23) Al_2O_3, Fe_2O_3 and CaO exhibit negative correlation with SiO_2, whereas Na_2O, K_2O and, to some extent, MgO do not define any definite trend. Ce, Zr, Y, Ni, Nb, Rb and Sr show no definite trend when plotted against SiO_2 (Figure 12(a)). In the normative Ab-An-Or diagram (Figure 24) of O' Conor [14], the gneisses plot in the trondhjemite, tonalite and granitic fields. This is also supported by the fact that on other normative diagrams such as

CaO-Na_2O-K_2O (Figure 25), the gneisses display their granitic-trondhjemite-tonalite nature. On the AFM diagram (Figure 26) of Irwin & Baragar (1971), gneisses display a typical calc-alkaline trend. Since these rocks are slightly alkaline rich, the majority of plots fall near the alkali apex. On the A/NK vs A/CNK diagram of Maniar and Piccoli (1989) (Figure 27) the plots fall in the peraluminous field. On the SiO_2 vs TiO_2 diagram (Figure 28) the plots fall in the orthogneiss field, indicating the igneous origin of the precursors.

Trace element values are variable, with Sr ranging from 61 to 464 ppm, Zr from 60 to 117 ppm, and Y from 15.5 to 117 ppm. Higher concentrations of Zr in a few samples are attributed to the presence of appreciable amounts of modal zircon. Yttrium in the gneisses ranges from 15 to 26 ppm except for two samples, which show values of 70 and 117 ppm. The Ce/Y ratio ranges between 0.44 and 5.08 ppm. Zr ranges from 60 to 117 and Nb from 10 to 33 ppm. Ce/Y vs Y is shown in Figure 29, and the plots show a negative trend. Ce/Y values for the gneisses of the present study are similar to the reported values for the Archaean gneisses (Gill, [15]). The plot shows a positive trend. On the K/Rb vs Rb/Sr diagram (Figure 30), the plots show a negative trend. SiO_2 vs trace elements like Sr and Rb are shown in Figure 31, and the Sr plots show a negative trend while the Rb plots show a positive trend.

The gneisses have moderate to high contents of LIL elements (K, Rb, Cs, Th, and U), show low K/Rb ratios (98.54 - 262.82) with an average of 156.57, and high Rb/Sr ratios (0.13 - 7.72). High field strength (HFS) elements (Ti, Nb, Zr, Ta, Hf, and Y) and transition elements (Ni, Cr, Co, V, and Sc) show considerable variation. The REE patterns are highly fractionated with $(La/Yb)_N$ ratios ranging from 19 to 2 and are similar to REE patterns observed in Archaean grey gneisses across the world [2] [16]. All the samples show a depleted Eu pattern, indicating the role of plagioclase in fractional crystallization.

Nine samples of gneisses have been analyzed for rare earth elements. The REE data is presented in Table 3, and the chondrite-normalized REE patterns are shown in Figure 32. The chondrite-normalized values are from Taylor and McLennan (1985).

The major and trace elemental compositions and CIPW calculations of granites are listed in Tables 6-8. SiO_2 content ranges from 71.63 to 75.74%, with an average of 73.6%. Al_2O_3 ranges from 12.93 to 14.2%, with an average of 13.73%. Fe_2O_3 ranges from 0.66 to 3.20%, with a mean value of 1.67%. MgO contents are low, varying from 0.05 to 0.35%, with an average of 0.2%. CaO ranges from 0.73 to 1.51%, with a mean value of 1.02%. Na_2O ranges from 3.05 to 4.26%, with an average of 3.71%, and K_2O shows relatively higher values, ranging from 3.63 to 6.42%, with a mean of 5.08%.

Major oxides plotted on Harker's variation diagram (Figure 33) show a systematic decrease in CaO, Fe_2O_3, Al_2O_3, and Na_2O with increasing SiO_2, while K_2O exhibits an increasing trend. MgO displays little to no variation with SiO2, indicating its limited mobility during magmatic differentiation.

On the Ab-An-Or diagram (Figure 34) after O'Conor [14] and CaO-Na_2O-K_2O

diagram (Figure 35) after Hunter *et al.*, [17], the samples plot within the well-defined granite field. On the AFM diagram (Figure 36) of Irwin & Baragar (1971), granites display a typical calc-alkaline trend. The granites are predominantly peraluminous in nature, as confirmed by the A/NK vs A/CNK diagram (Figure 37) after Manior and Piccoli (1989), where all the plots fall in the peraluminous field. The ratio varies from 1.3 to 1.7, with an average of 1.5, which suggests that the granites represent late-phase differentiates of the granitic magma.

Table 1. Major element analysis of gneisses.

Sample No	AT1	AD1	GH1	HG1	HG2	TU2	CO1	CG1	HG3
SiO_2	63.49	74.93	74.54	75.17	75.03	73.96	71.43	72.35	69.24
Al_2O_3	14.53	13.46	13.91	13.28	13.37	13.53	16.49	15.23	15.35
Fe_2O_3	6.91	0.75	1.25	1.02	1.77	1.89	0.63	1.42	4.63
MgO	2.67	0.17	0.14	<0.05	0.2	0.35	0.24	0.42	1.18
CaO	4.43	0.75	0.79	0.73	0.92	1.3	3.01	2.08	1.68
Na_2O	4.46	3.96	3.62	3.89	3.89	3.63	5.92	5.55	4.98
K_2O	1.73	4.8	4.57	5.26	4.08	4.18	0.98	1.66	0.41
TiO_2	0.86	0.1	0.12	0.08	0.16	0.27	0.06	0.22	0.02
P_2O_5	0.25	<0.05	<0.05	<0.05	<0.05	<0.05	<0.05	<0.05	<0.05
MnO	0.08	<0.05	<0.05	<0.05	<0.05	<0.05	<0.05	<0.05	0.25
Cr_2O_3	<0.05	<0.05	<0.05	<0.05	<0.05	<0.05	<0.05	<0.05	<0.05
BaO	<0.05	<0.05	<0.05	<0.05	<0.05	0.07	<0.05	<0.05	<0.05
LOI	0.48	0.55	0.52	0.45	0.44	0.69	0.43	0.31	1.42
Total	99.89	99.47	99.46	99.88	99.86	99.87	99.19	99.24	99.16
$Na_2O + K_2O$	6.19	8.76	8.19	9.15	7.97	7.81	6.9	7.21	5.39
$Fe_2O_3 + MgO$	9.58	0.92	1.39	1.07	1.97	2.24	0.87	1.84	5.81

Table 2. Trace element analysis of gneisses.

Sample No	AT1	AD1	GH1	HG1	HG2	TU2	CO1	CG1	HG3
Sr	181	52	52	51	57	150	531	464	245
Zr	108	60	78	69	110	117	93	63	112
V	99	<5	<5	<5	6	17	51	45	41
Sn	<50	<50	<50	<50	<50	<50	<50	<50	<50
Mo	0.79	<0.5	<0.5	1.02	<0.5	0.65	<0.5	1.08	0.5
Ga	23.14	32	21.84	20.42	21.37	16.71	22.19	23.14	20.42

Continued

Y	69.99	17.45	15.5	26.6	17.45	22.18	20.1	20.3	117
Nb	33.38	19.01	27.04	10.46	26.72	10.67	20.08	20.64	22.87
Th	19.28	22	27.99	17.06	36.31	18.74	17.43	28.12	17
Cu	<5	<5	<5	<5	<5	<5	<5	<5	<5
Pb	7	34	28	33	27	12	29	23	19
Zn	104	40	38	30	53	38	29	64	57
Ni	43	<5	<5	<5	<5	5	<5	<5	<5
U	3.78	4.92	3.46	9.1	4.72	1.98	4.91	4.7	9
Co	40.85	40.36	38.03	37.65	42.89	35.38	42.24	37.9	36.58
Cd	<0.5	<0.5	<0.5	<0.5	<0.5	<0.5	<0.5	<0.5	<0.5
Cs	3.16	1.73	2.06	1.64	2.57	1.73	1.65	1.72	2.53
Sb	<0.5	<0.5	<0.5	<0.5	<0.5	<0.5	<0.5	<0.5	<0.5
Bi	0.95	<0.5	<0.5	<0.5	<0.5	<0.5	<0.5	<0.5	<0.5
Ag	<1	<1	<1	<1	<1	<1	<1	<1	<1
Rb	146.3	401.28	283.6	239.6	265.59	136.6	70	132	13
K	1.44	4	3.81	4.38	3.4	3.48	0.82	1.38	0.34

Table 3. Rare earth element concentration of gneisses.

Sample No	AT1	AD1	GH1	HG1	HG2	TU2	CO1	CG1	HG3
La	36.77	32.65	40.5	31.82	43.5	53.28	33.32	32.11	43.3
Ce	77.03	64.33	78.85	31.82	31.79	87.99	62.01	66.83	51
Nd	37.87	22.87	28.13	11.8	11.82	31.51	11.82	28.12	31.84
Sm	8.91	5.1	5.82	2.7	2.72	6.8	2.7	5.1	6.9
Eu	1.21	<0.5	<0.5	<0.5	<0.5	<0.5	<0.5	<0.5	<0.5
Tb	1.53	0.62	0.67	0.5	0.57	0.73	0.5	0.7	0.65
Yb	8.45	3.33	1.48	3.41	3.47	1.78	3.31	3.65	3.86
Lu	1.13	0.52	<0.5	<0.5	<0.5	<0.5	<0.5	<0.5	<0.5
Ce/Y	1.10	3.69	5.09	1.20	1.82	4.67	3.09	3.29	0.44
K/Rb	98.54	99.68	134.29	182.94	128.02	255	116.67	104.8	262.82
Rb/Sr	0.81	7.72	5.45	4.7	4.66	0.91	0.13	0.28	0.05

Table 4. CIPW norm calculation of gneissic rocks.

Sample No	AT1	AD1	GH1	HG1	HG2	TU2	CO1	CG1	HG3
Quartz	19.5	32.07	34.55	31.05	34.84	33.96	26.89	29.07	34.34
Orthoclase	10.28	28.66	27.24	31.2	24.23	24.88	5.85	9.93	2.48
Albite	37.99	33.85	30.97	34.86	33.09	30.97	50.69	47.39	43.15
Anorthite	14.6	3.45	3.65	3.25	4.24	6.18	14.76	10.09	8.21
Corundum	-	0.5	1.69	-	1.01	0.8	0.35	0.65	3.88
Diopside	2.49	-	-	-	-	-	-	-	-
Hypersthene	5.5	0.42	0.35	0.12	0.5	0.87	0.6	1.05	3.01
Ilmenite	0.17	0.17	0.11	0.11	0.11	0.11	0.11	0.11	0.04
Apatite	0.58	0.12	0.12	0.12	0.12	0.12	0.12	0.12	0.12
Titanite	1.91	-	-	0.03	-	-	-	-	-
Hematite	6.95	0.76	1.26	1.02	1.08	1.91	0.64	1.43	4.67
Rutile	-	0.01	0.06	0.01	0.1	0.21	-	0.16	-

Table 5. Major elements of granites.

(a)

Sample No.	MB1	MB2	HG4	GB1	AH1	MN1	AM1	KR1
SiO_2	73.39	71.63	73.78	74.41	73.91	74.63	73.03	71.63
Al_2O_3	13.99	14.05	13.92	13.56	13.5	13.41	13.74	14.2
Fe_2O_3	1.85	3.2	1.11	1.32	1.74	1.32	1.93	3.14
MgO	0.24	0.56	0.13	0.15	0.35	0.14	0.05	0.05
CaO	1.03	1.17	0.73	0.95	0.98	0.93	0.91	1.51
Na_2O	3.85	3.53	3.13	3.6	3.62	3.53	3.35	4.14
K_2O	4.74	4.85	6.42	5.23	4.79	5.14	5.12	3.63
TiO_2	0.2	0.34	0.12	0.13	0.25	0.14	0.27	0.33
P_2O_5	0.06	0.08	<0.05	<0.05	<0.05	<0.05	0.07	0.08
MnO	<0.05	<0.05	<0.05	<0.05	<0.05	<0.05	<0.05	<0.05
Cr_2O_3	<0.05	<0.05	<0.05	<0.05	<0.05	<0.05	<0.05	<0.05
BaO	<0.05	0.06	0.06	0.05	<0.05	0.07	0.1	0.05
LOI	0.56	0.46	0.52	0.49	0.7	0.56	1.04	0.65
Total	99.91	99.93	99.92	99.89	99.84	99.87	99.61	99.41
$Na_2O + K_2O$	8.59	8.38	9.55	8.83	8.41	8.67	8.47	7.77

Continued

(b)								
Sample No.	KR2	KG1	GR1	DB2	DD3	DD7	CO2	MN2
SiO_2	72.75	74.59	75.09	73.78	72.76	75.74	72.19	74.31
Al_2O_3	14.6	13.65	13.01	13.61	14.16	12.95	14.47	12.93
Fe_2O_3	1.22	1.13	1.69	1.26	1.37	0.66	1.92	1.91
MgO	0.2	0.11	0.19	0.21	0.19	0.05	0.31	0.27
CaO	1.13	0.9	0.78	1.15	0.88	0.83	1.53	0.94
Na_2O	3.87	4.1	3.05	3.99	4.25	3.48	4.26	3.57
K_2O	5.1	4.7	5.44	5.31	5.61	5.58	4.43	5.21
TiO_2	0.14	0.1	0.15	0.16	0.13	<0.05	0.21	0.18
P_2O_5	<0.05	<0.05	<0.05	<0.05	<0.05	<0.05	0.1	<0.05
MnO	<0.05	<0.05	<0.05	<0.05	<0.05	<0.05	<0.05	<0.05
Cr_2O_3	<0.05	<0.05	<0.05	<0.05	<0.05	<0.05	<0.05	<0.05
BaO	0.08	<0.05	<0.05	0.08	<0.05	<0.05	<0.05	<0.05
LOI	0.81	0.62	0.46	0.37	0.52	0.6	0.47	0.54
Total	99.9	99.9	99.86	99.92	99.87	99.89	99.89	99.86
$Na_2O + K_2O$	8.97	8.8	8.49	9.3	9.86	9.06	8.69	8.78

Table 6. Trace element analysis of granites.

Sample No.	MB1	MB2	HG4	GB1	AH1	MN1	AM1
Sr	79	99	172	102	102	122	138
Zr	146	165	38	92	113	96	135
V	7	13	9	32	16	5	19
Sn	<50	<50	<50	<50	<50	<50	<50
Mo	0.5	<0.5	1.25	<0.5	0.71	7.76	<0.5
Ga	20.67	22.32	15.52	19.31	18.36	17.88	15.79
Y	13.82	25.84	9.1	11.49	36.94	28.12	14.52
Nb	22.56	24.95	8.49	11.96	18.62	8.37	9.09
Cu	23	<5	<5	7	<5	<5	<5
Pb	26	26	21	32	15	26	20
Zn	52	73	24	32	36	30	33
Ni	<5	<5	<5	<5	6	<5	23

Continued

Co	35.38	35.95	48	43.43	46.89	53.58	26.92
Cd	<0.05	<0.5	<0.5	<0.5	<0.5	<0.5	<0.5
Sb	<0.05	<0.5	<0.5	<0.5	<0.5	<0.5	<0.5
Bi	<0.05	<0.05	<0.05	<0.05	<0.05	<0.05	<0.05
Ag	<1	<1	<1	<1	<1	<1	<1
Rb	241.92	262.14	190.31	227.34	176.88	215.14	135.12
K	3.95	4.04	5.35	4.36	3.99	4.28	4.27

Table 7. Rare earth element analysis of granites.

Sample No.	MB1	MB2	HG4	GB1	AH1	MN1	AM1
La	72.22	40.78	23.44	39.82	50.13	23.36	66.07
Ce	172.72	79.31	46.35	76.28	96.08	43.3	121.54
Nd	45.49	27.4	16.77	26.12	33.63	14.92	34.08
Sm	8.04	5.44	3.11	4.58	6.62	3.1	5.01
Eu	0.62	0.71	0.56	0.67	0.72	0.6	0.76
Tb	0.73	0.85	0.5	0.51	0.94	0.6	0.5
Yb	0.96	2.46	0.78	1.19	3.85	2.86	1.45
Lu	0.5	0.5	0.5	0.5	0.53	0.5	0.5
Ce/Y	12.50	3.07	5.09	6.64	2.60	1.54	8.37
K/Rb	0.02	0.02	0.03	0.02	0.02	0.02	0.03
Rb/Sr	3.06	2.65	1.11	2.23	1.73	1.76	0.98

Table 8. CIPW norm calculation of granites.

Sample No.	MB1	MB2	HG4	GB1	AH1	MN1	AM1	KR1
Quartz	30.65	29.42	29.54	31.49	32.26	32.61	32.56	30.88
Orthoclase	28.19	28.66	38.18	31.08	28.54	30.55	30.73	21.75
Albite	32.75	29.87	26.65	30.63	30.89	30.04	28.77	35.45
Anorthite	4.77	5.29	3.3	4.44	4.59	4.34	4.24	7.27
Corundum	0.79	1.06	0.62	0.35	0.69	0.47	1.17	0.84
Hypersthene	0.6	1.39	0.32	0.37	0.87	0.35	0.12	0.12
Ilmenite	0.11	0.11	0.11	0.11	0.11	0.11	0.11	0.11
Apatite	0.14	0.18	0.12	0.12	0.12	0.12	0.12	0.12

Continued

Hematite	1.86	3.2	1.12	1.33	1.75	1.33	1.96	0.12
Rutile	0.14	0.28	0.06	0.07	0.19	0.08	0.21	0.27

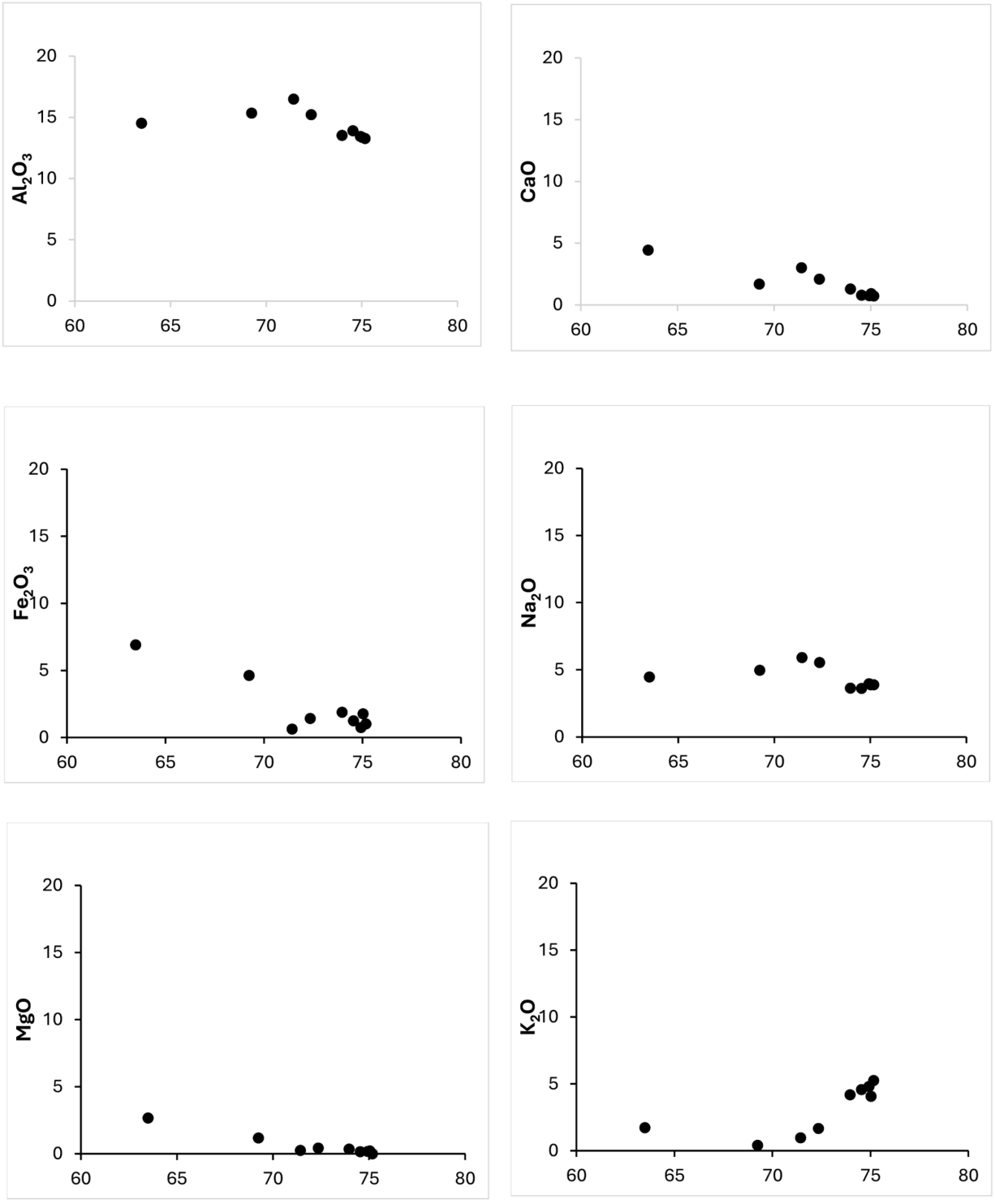

Figure 23. Harker's variation diagram of gneisses.

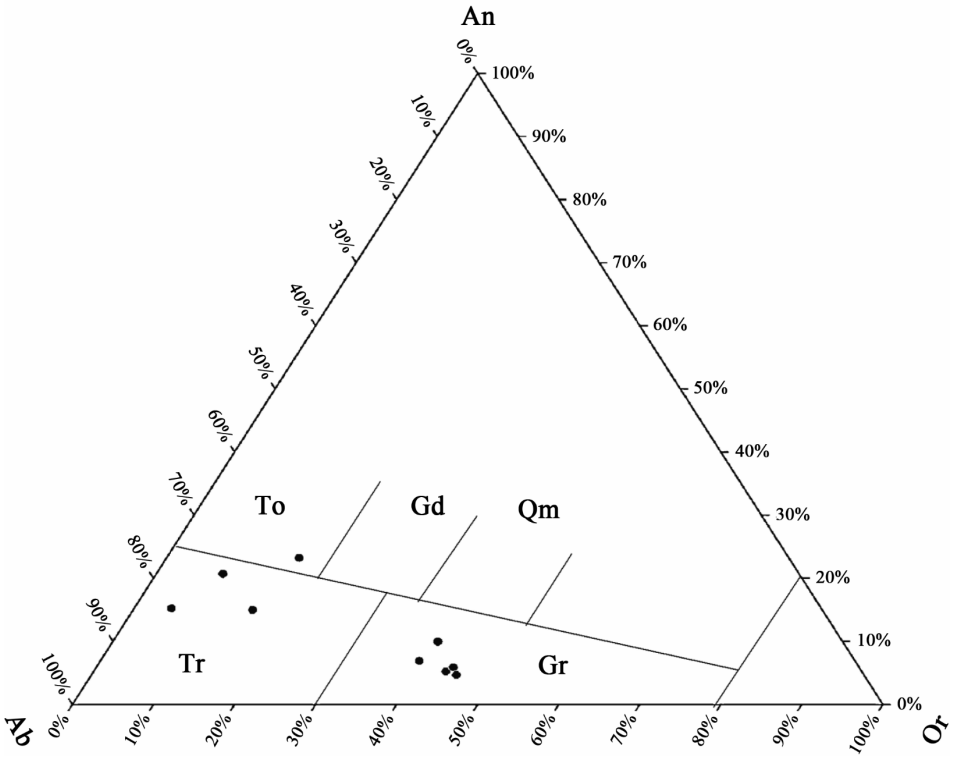

Figure 24. Ab-An-Or diagram of gneiss after O'Conor (1965). Note that the plots fall in the trondhjemite, tonalite, and granite fields.

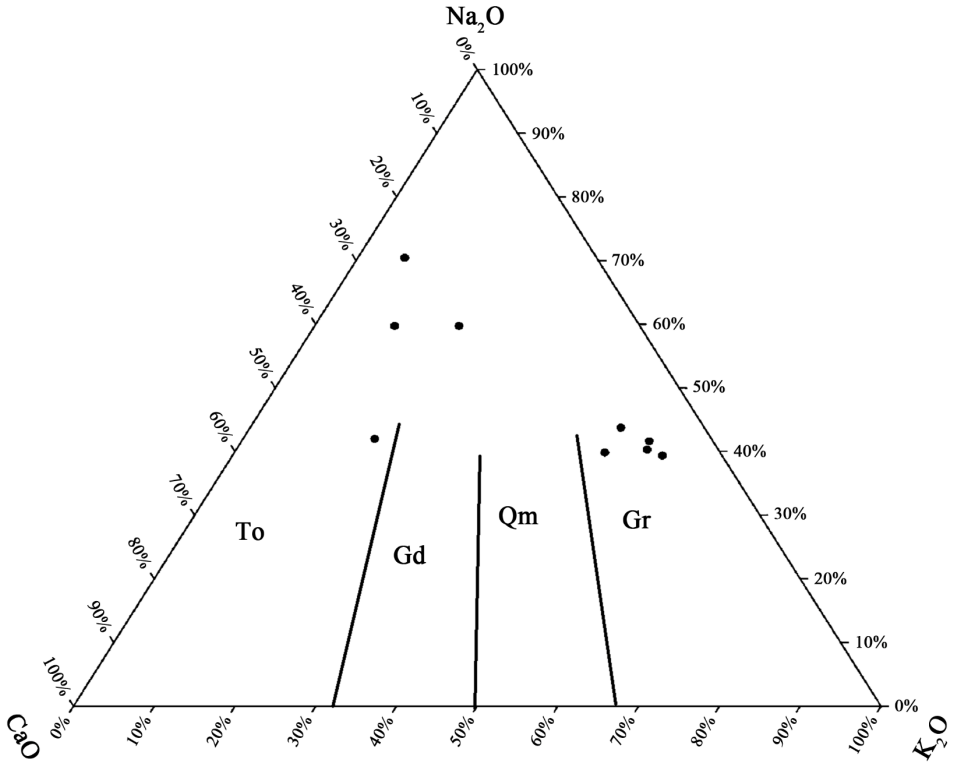

Figure 25. CaO-Na_2O-K_2O diagram of gneiss after Hunter *et al.* (1978); the plots fall in the granodiorite, tonalite, and granite fields.

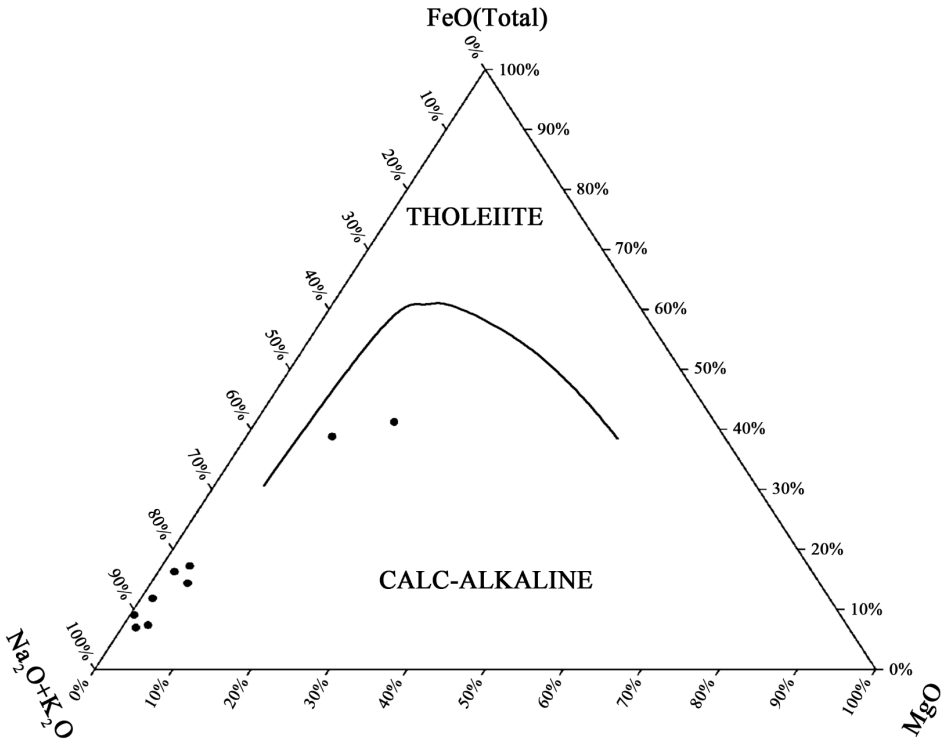

Figure 26. AFM diagram for gneiss after Irwin & Baragar (1971); the plots fall along the calc-alkaline trend.

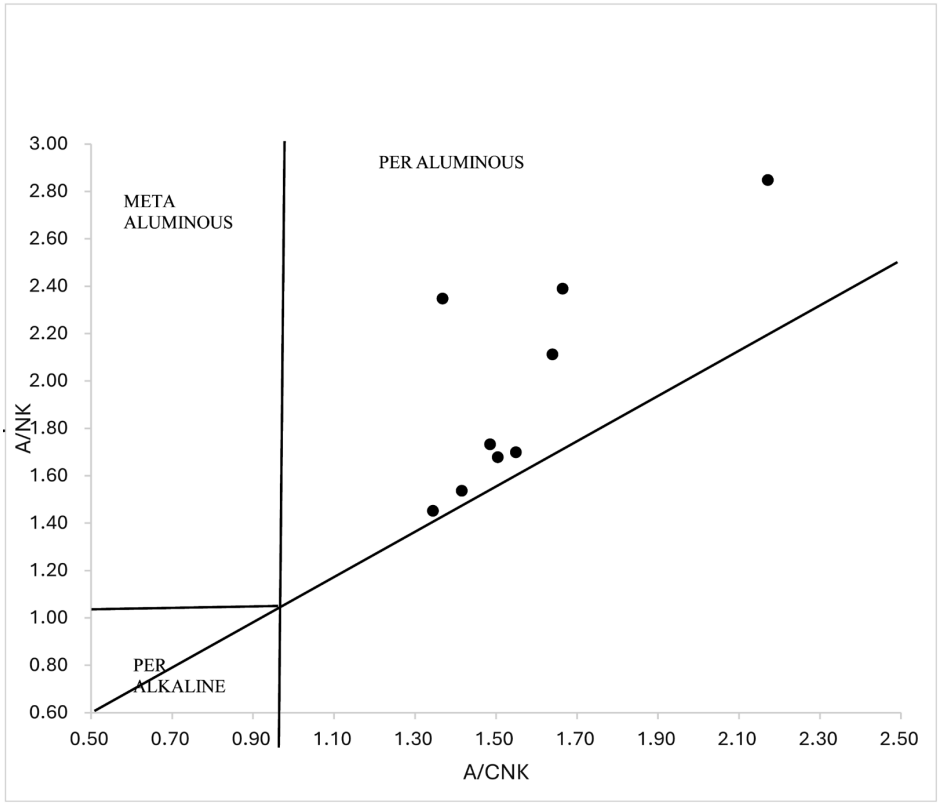

Figure 27. A/NK vs A/CNK diagram of gneiss after Manior and Piccoli (1989), all the plots fall in the peraluminous field.

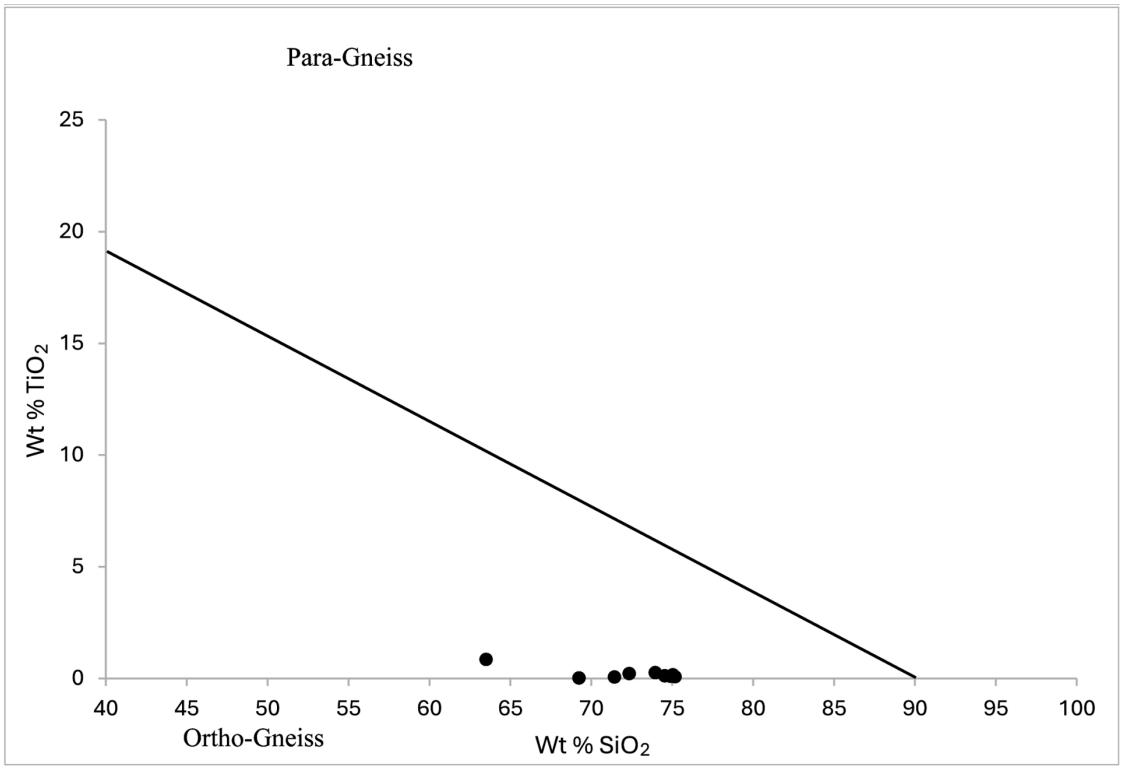

Figure 28. SiO_2-TiO_2 diagram after Torney (1976), all the plots fall in the orthogneiss field.

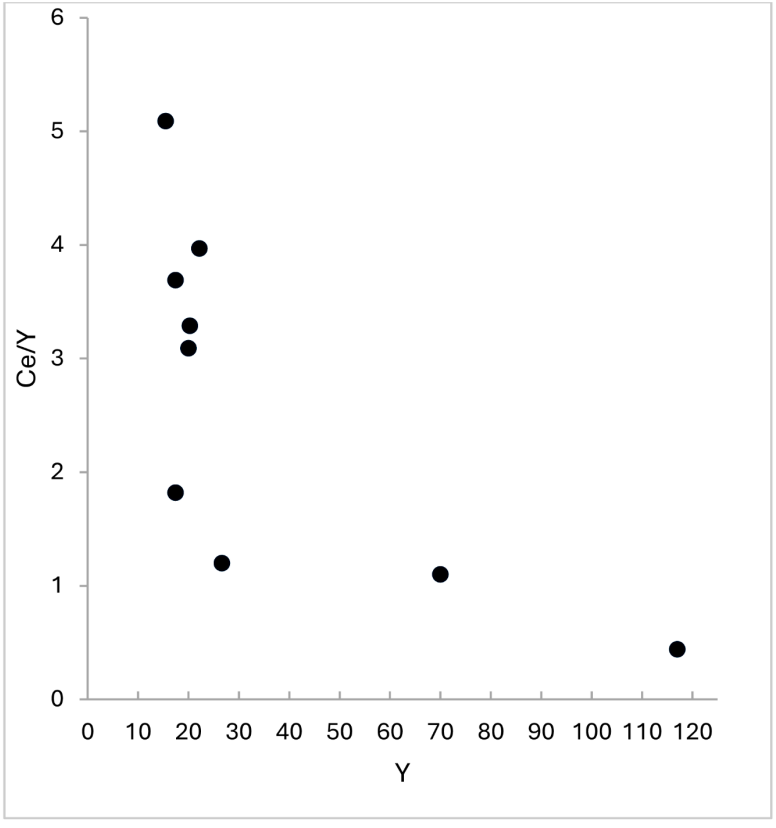

Figure 29. Ce/Y vs. Y for the gneiss.

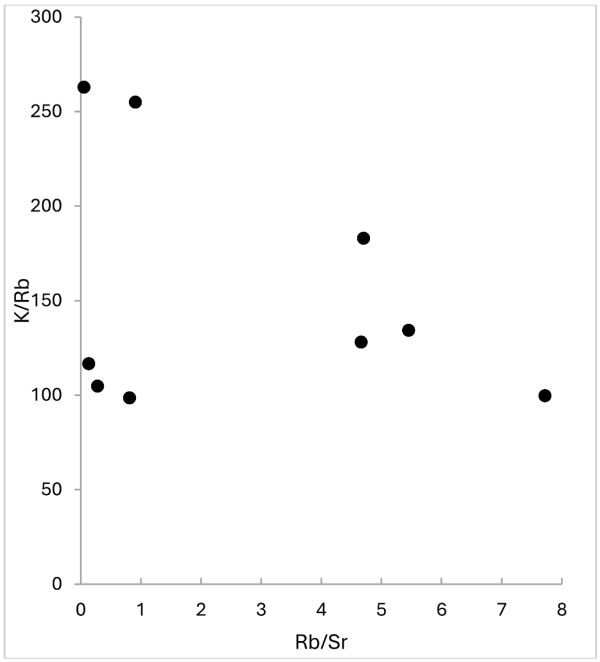

Figure 30. K/Rb vs. Rb/Sr diagram for the gneiss.

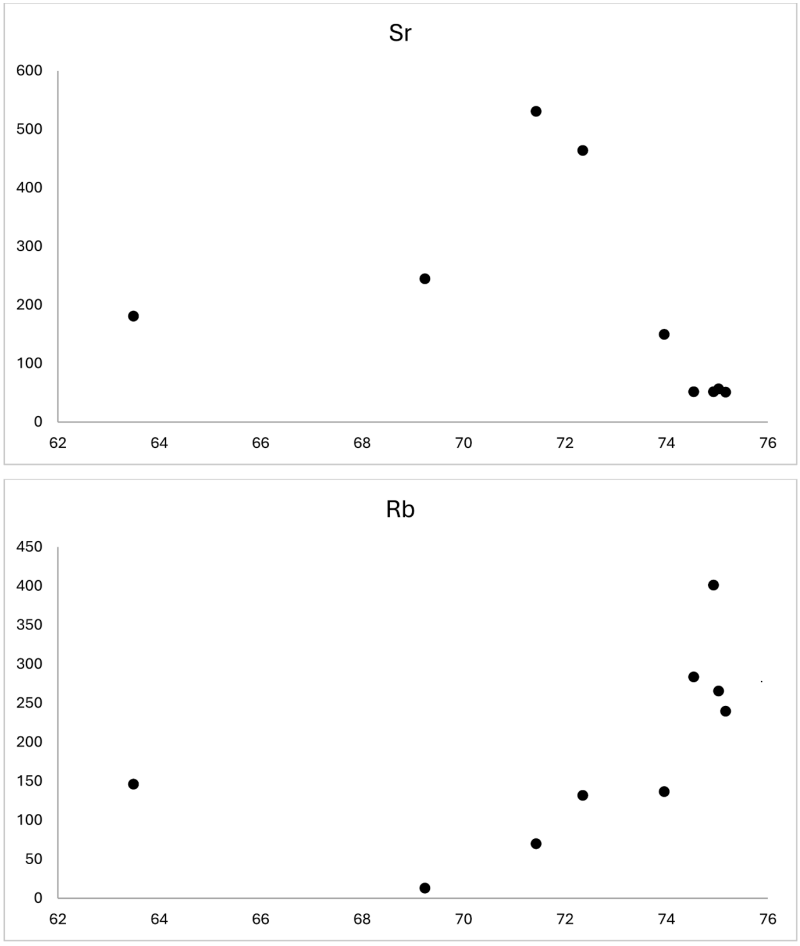

Figure 31. SiO_2 vs. Sr and Rb diagram for gneiss.

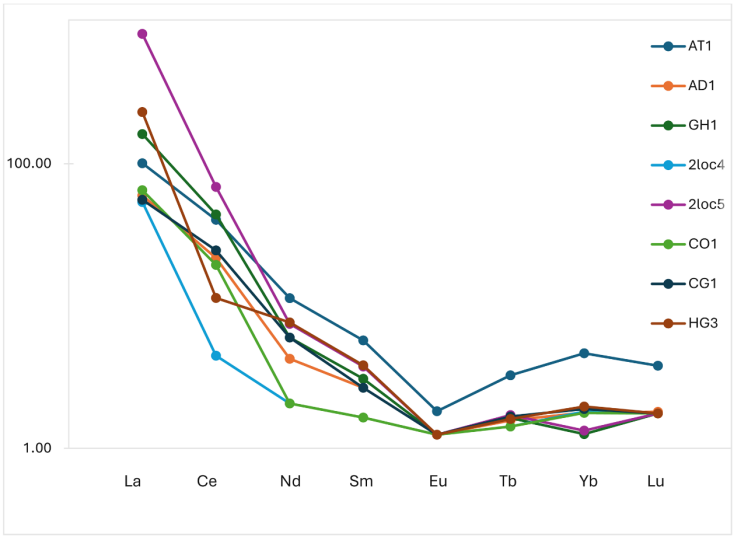

Figure 32. Rare earth element pattern for gneisses.

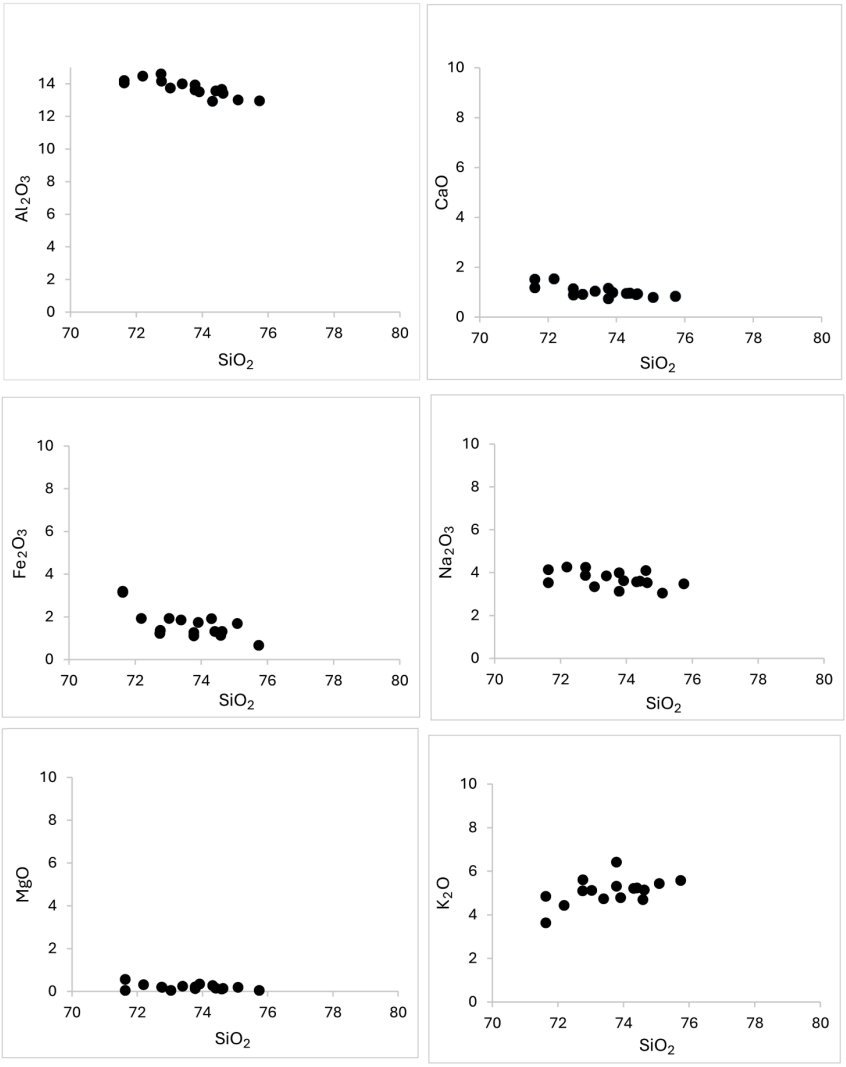

Figure 33. Harker's variation diagram for granites.

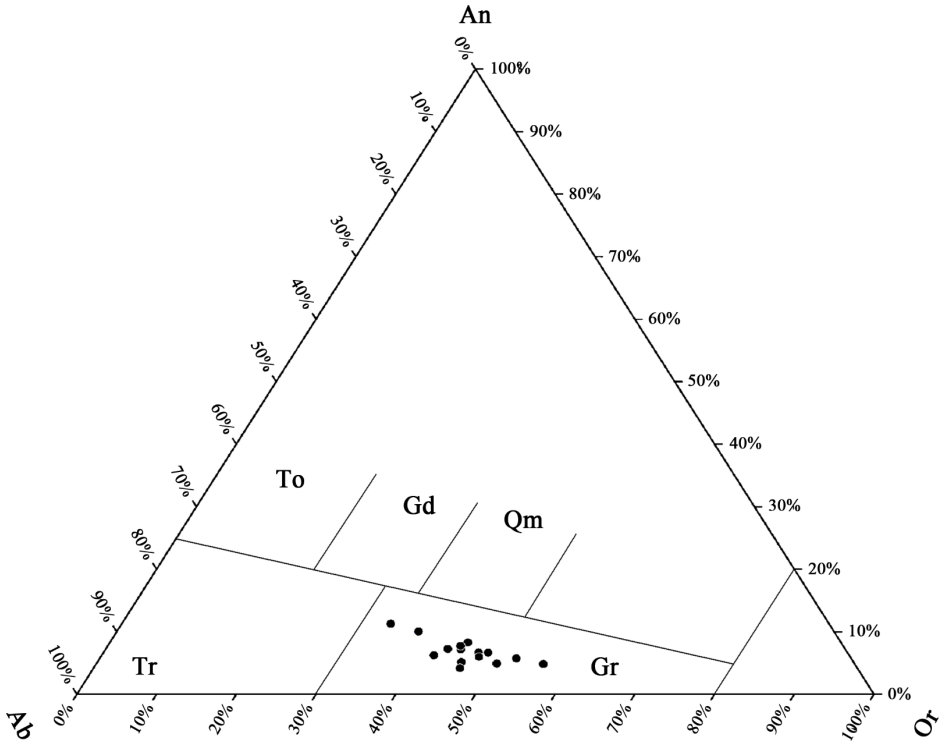

Figure 34. Ab-An-Or diagram of granites after O'Conor (1965); all the plots fall in the granite fields.

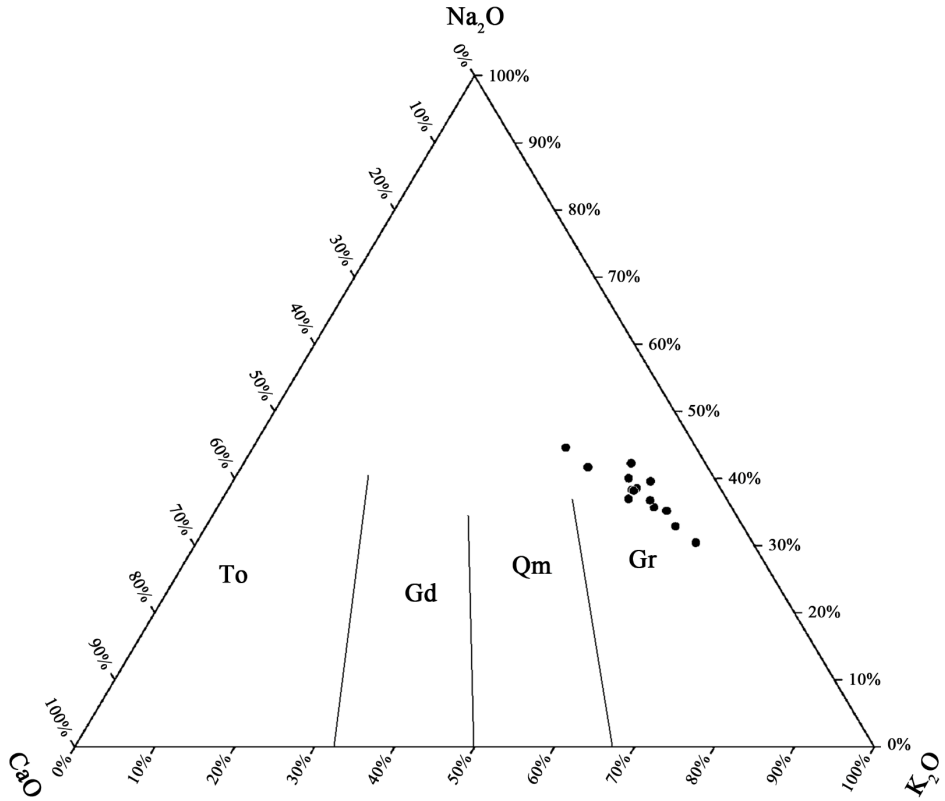

Figure 35. CaO-Na_2O-K_2O diagram after Hunter *et al.* (1978), all the plots fall in the granite field.

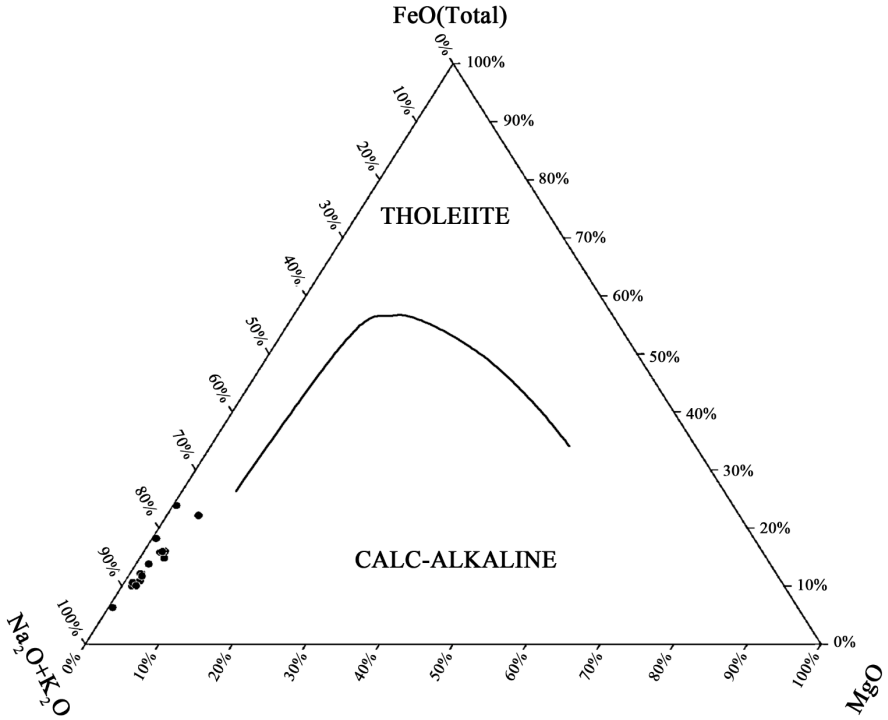

Figure 36. AFM diagram for granites after Irwin & Baragar (1971), the plots fall along the calc-alkaline trend.

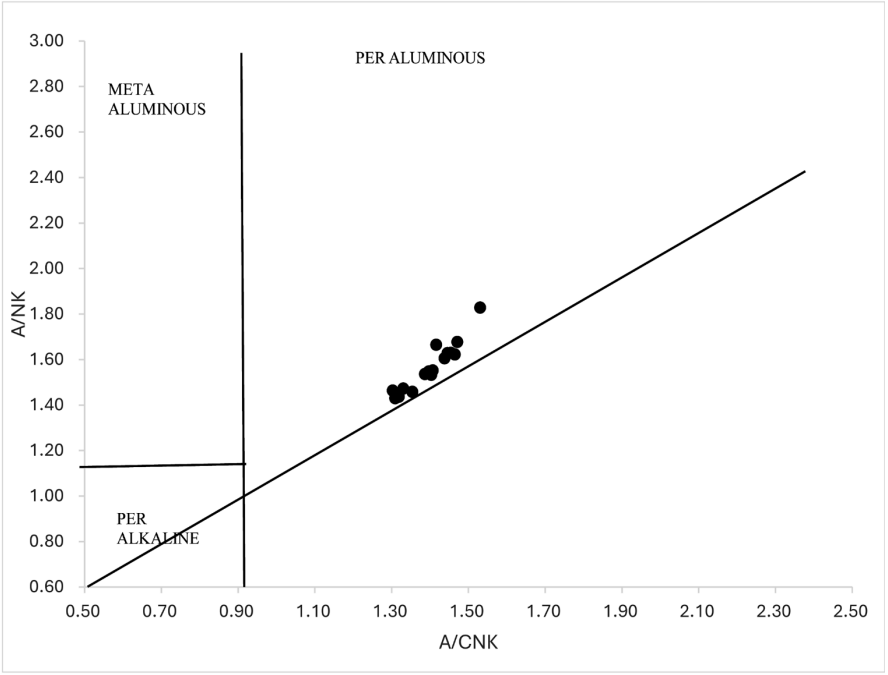

Figure 37. A/NK vs A/CNK diagram after Maniar and Piccoli (1989), all the plots fall in the peraluminous field.

Trace element concentrations show considerable variation, with Sr ranging from 79 to 172 ppm, Zr ranging from 38 to 165 ppm, and Y from 9.1 to 36.94 ppm. The granites are characterized by very low K/Rb ratios (0.02 to 0.03) and Rb/Sr

ratios (0.98 to 3.06).

The Ce/Y ratios vary from 1.54 to 12.50 ppm. On the Ce/Y vs Y diagram (Figure 38), plots show a negative trend for the granites. The K/Rb vs Rb/Sr relationship is shown in Figure 39, and the plots show a negative trend. Variations of SiO_2 against the trace elements Sr and Rb are presented in Figure 40, Sr plots show a positive trend and Rb plots show a negative trend.

Seven samples of granite were analyzed for rare earth elements, and the REE data are presented in Table 7. Chondrite-normalized REE patterns, based on normalization values of Taylor and McLennan (1985), are shown in Figure 41. Granites exhibit moderate to high total REE abundances with low HREE. The REE patterns are highly fractionated, with $(La/Yb)_N$ ratios ranging from approximately 50 to 5. All samples display a pronounced depleted Eu anomaly, indicating the significant role of plagioclase in fractional crystallization. On the K_2O vs Na_2O diagram (Figure 42) after Harpun (1963), the plots fall in S-Type and A-Type granite fields.

Tectonic discrimination diagrams were constructed using selected trace element ratios to constrain the tectonic setting of the granitoids. Standard discrimination plots including Rb vs (Y + Nb), Nb vs Y, and Ta vs Yb after Pearce *et al.* [18] were employed. Trace element values reported below the detection limit (Ta < 0.5 ppm) were plotted using the detection limit value. On the Rb vs (Y + Nb) diagram (Figure 43), most samples plot within the volcanic arc granite (VAG) to syn-collisional granite (Syn-COLG) fields. The Nb vs Y diagram (Figure 44) shows clustering of samples within the arc-related field. The Ta vs Yb diagram (Figure 45) further confirms that all samples fall within the arc-related granitoid field.

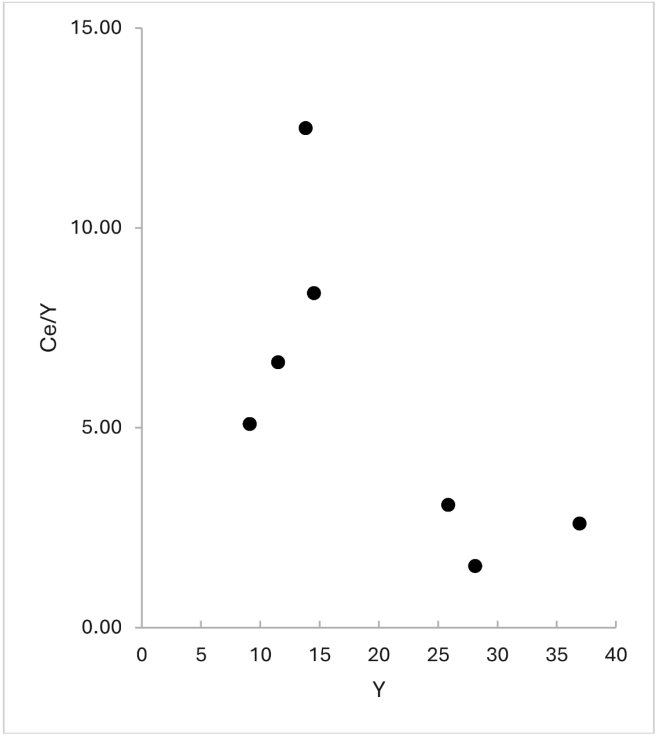

Figure 38. Ce/Y vs. Y diagram for the granite.

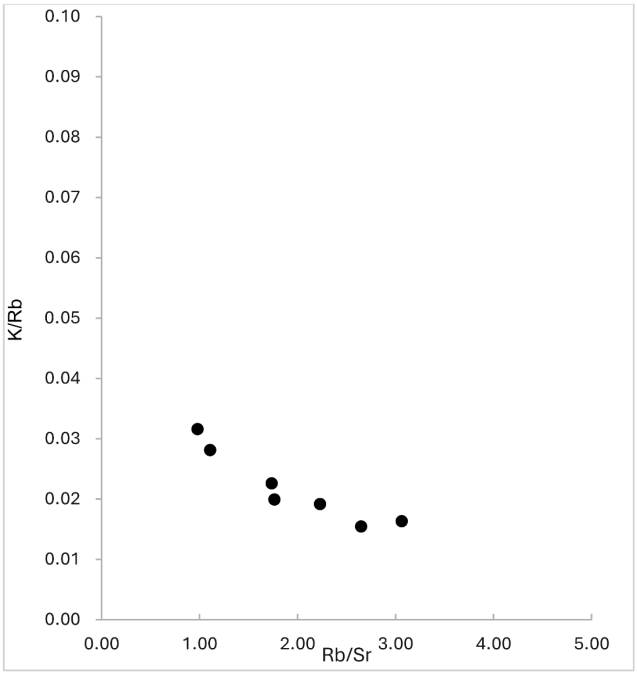

Figure 39. K/Rb vs Rb/Sr diagram for the granite.

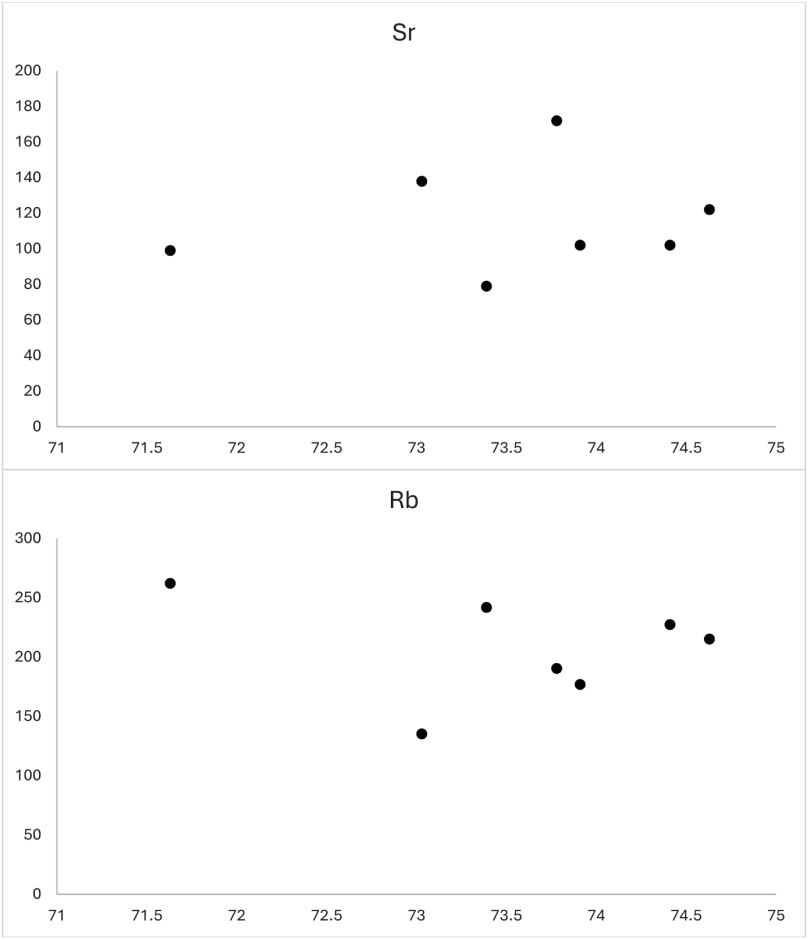

Figure 40. SiO_2 vs. Sr and Rb diagram for granite.

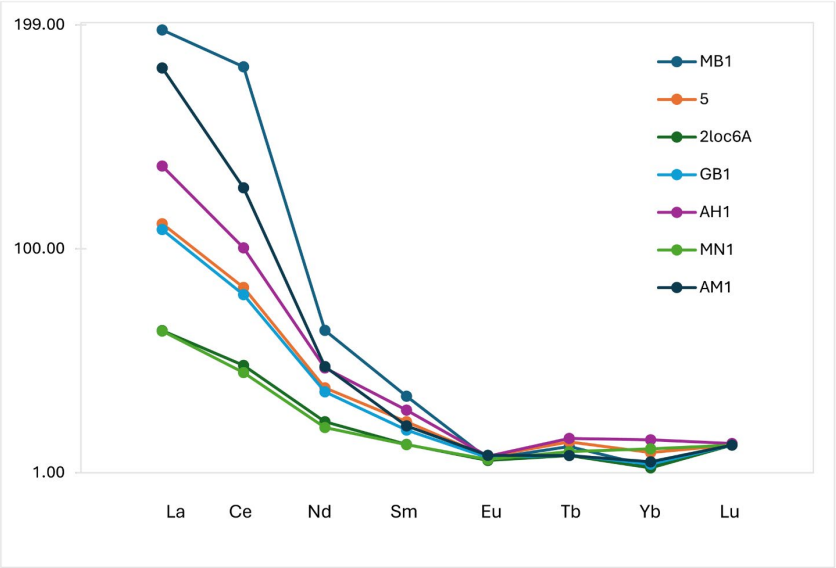

Figure 41. Rare earth element pattern for granites.

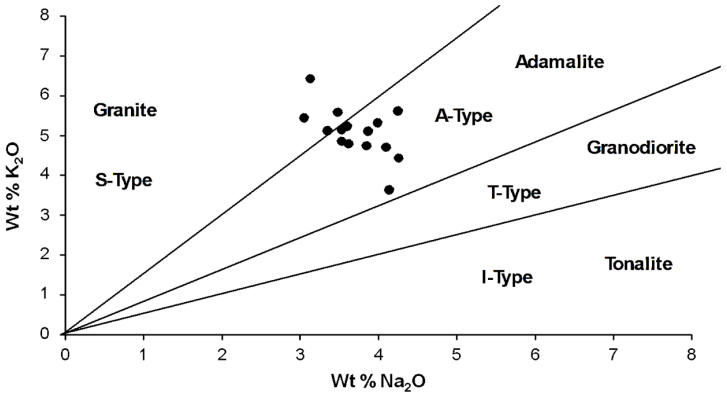

Figure 42. K_2O vs. Na_2O diagram after harpun (1963).

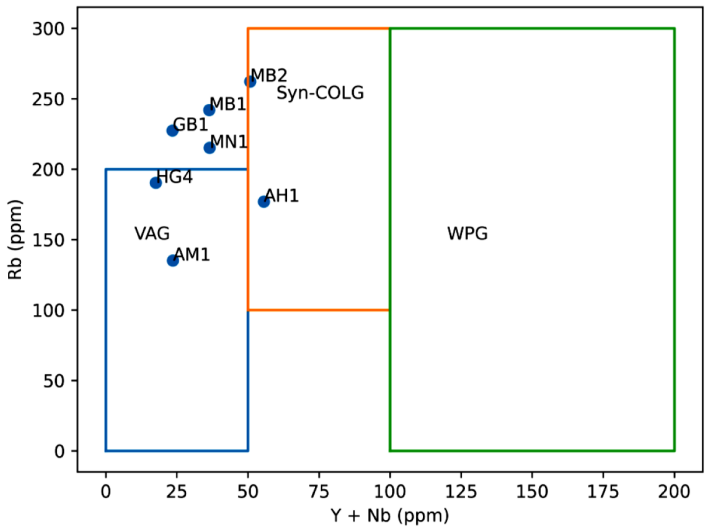

Figure 43. Rb vs (Y + Nb) tectonic discrimination diagram for granites from the Devanahalli area after Pearce *et al.* (1984). Most samples plot within the VAG to Syn-COLG fields.

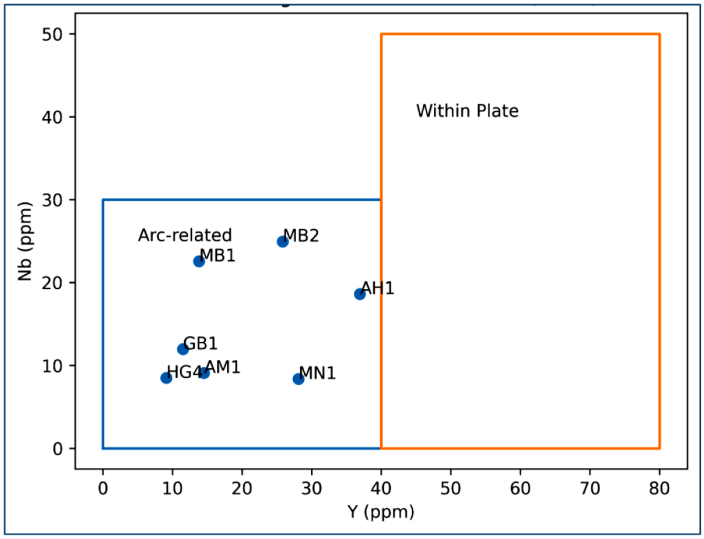

Figure 44. Nb vs Y tectonic discrimination diagram for granites from the Devanahalli area after Pearce *et al.* (1984), showing arc-related affinity.

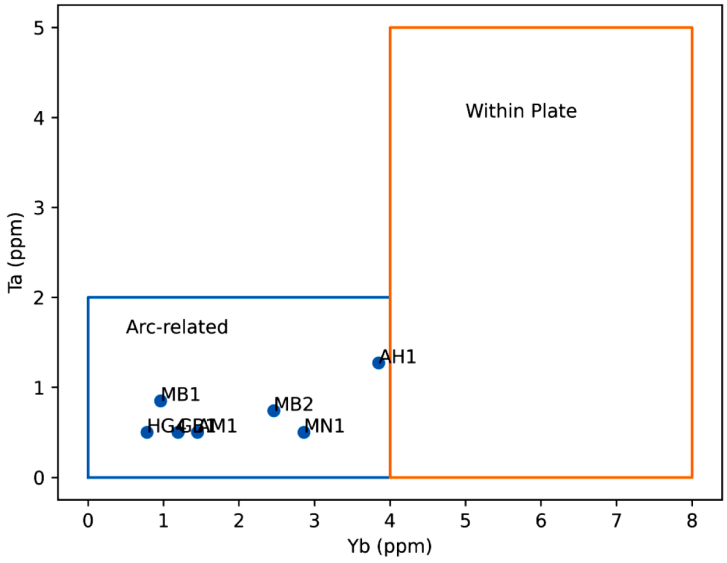

Figure 45. Ta vs Yb tectonic discrimination diagram for granites from the Devanahalli area after Pearce *et al.* (1984). All samples plot in the arc-related field.

7. Discussion

7.1. Integration of Field, Petrographic, and Geochemical Characteristics

The field relationships observed in the Devanahalli area provide important constraints on the relative timing and evolution of lithological units. The gneisses occur as foliated, banded, streaky, and migmatitic varieties, recording multiple stages of deformation and partial melting, while the granites intrude the gneissic fabric, indicating their younger emplacement. The presence of migmatitic structures such as schollen, stromatic, and ptygmatic banding strongly suggests in situ partial melting of the gneissic crust.

Petrographic evidence supports this interpretation. The gneisses preserve high-grade deformation microstructures such as undulose extinction in quartz, recrystallized grain boundaries, myrmekitic textures, and mineral alignment defining foliation, consistent with amphibolite- to granulite-facies metamorphism. The granites, on the other hand, display dominantly magmatic textures but locally preserve evidence of deformation and hydrothermal overprinting, indicating emplacement during the late stages of tectono-thermal evolution.

Geochemically, the gneisses exhibit tonalitic-trondhjemitic to granodioritic compositions, calc-alkaline affinity, and peraluminous nature, consistent with TTG-type protoliths [2] [4] [5]. The granites are silica-rich, strongly peraluminous, and enriched in large ion lithophile elements, characteristics typical of crust-derived granitic melts. Thus, the field, petrographic, and geochemical datasets collectively suggest a coherent evolutionary history involving early crust formation followed by later crustal reworking. Major element variation trends suggest fractional crystallization involving plagioclase, K-feldspar, and biotite [19] [20]. Trace element signatures show enrichment in large-ion lithophile elements (LILE) and depletion in high-field-strength elements (HFSE), typical of continental crust-derived magmas [21] [22].

7.2. Genetic Relationship between Gneisses and Granites

The geochemical similarities between the gneisses and granites provide strong evidence for a genetic link between the two rock types. Both lithologies display peraluminous character, enrichment in light rare earth elements (LREEs), depletion in heavy rare earth elements (HREEs), and pronounced negative Eu anomalies. These features are typical of melts derived from feldspar-bearing crustal sources and reflect significant involvement of plagioclase during melting and fractionation [14] [21] [22].

The tonalitic-granodioritic composition of the gneisses, coupled with widespread migmatization observed in the field, indicates that these rocks likely represent fertile crust capable of undergoing partial melting. Gneisses consist of innumerable enclaves of mafic-ultramafic rocks, indicating their genetic relationship. The peraluminous nature of the granites, their high silica content, low MgO, and crust-like trace element signatures further support derivation through partial melting of older gneissic crust rather than from mantle-derived magmas.

Additionally, the occurrence of gneiss xenoliths within granitic bodies and the spatial association between migmatites and granites reinforce the interpretation that the granites represent anatectic melts derived from the local gneissic basement during late Archaean thermal events. Therefore, the data strongly support a model in which the granites were generated by partial melting of the pre-existing gneisses during crustal thickening and heating associated with craton stabilization.

7.3. Tectonic Implications

The geochemical signatures of both gneisses and granites, including calc-alkaline

affinity, enrichment in LILE, depletion in HFSE, and TTG-like characteristics of the gneisses, are consistent with formation in an Archaean convergent margin or subduction-related tectonic setting. Similar geochemical characteristics have been widely documented from the Dharwar Craton and other Archaean terrains worldwide.

The evolutionary sequence inferred for the Devanahalli area involves the formation of early TTG crust, high-grade metamorphism and deformation of the gneisses, partial melting and migmatization of the crust, and emplacement of late-stage crustally derived granites.

This multi-stage evolution reflects prolonged crustal growth and reworking processes associated with the stabilization of the eastern Dharwar Craton during the late Archean.

To constrain the tectonic setting of the granitoids, tectonic discrimination diagrams after Pearce *et al.*, [17] were used. These results indicate that the granitoids were emplaced in a convergent tectonic regime and derived predominantly from partial melting of older continental crust during Neoarchean crustal reworking of the eastern Dharwar Craton.

8. Conclusions

1) The area of Devanahalli, Karnataka, is dominantly composed of the Peninsular Gneissic Complex (PGC), intruded by granites and associated with enclaves and lenses of mafic-ultramafic rocks, representing a polyphase Archaean crustal assemblage.

2) Field relationships indicate that the gneisses occur as foliated, banded, streaky, and migmatitic varieties, recording multiple episodes of deformation, partial melting, and metamorphism under amphibolite to granulite facies conditions. Granites intrude the gneissic fabric, indicating their younger emplacement during late Archaean tectonothermal events.

3) Petrographic studies reveal that gneisses are composed of quartz, plagioclase, K-feldspar, biotite, and hornblende, with well-developed gneissic foliation and deformation microstructures such as undulose extinction, recrystallization, and myrmekitic textures. These features confirm their igneous protoliths and subsequent modification by high-grade metamorphism.

4) Granites exhibit hypidiomorphic granular to porphyritic textures with mineral assemblages of quartz, K-feldspar, plagioclase, and biotite, along with accessory zircon, apatite, allanite, and sphene. Textural and mineralogical characteristics indicate a dominantly magmatic origin with later deformation and hydrothermal overprinting in localized zones.

5) Geochemical data show that the gneisses have tonalitic-trondhjemitic to granodioritic compositions with calc-alkaline affinity and peraluminous nature, consistent with TTG-type magmatism. Their major and trace element characteristics support derivation from partial melting of basaltic to amphibolitic sources.

6) Chondrite-normalized REE patterns of the gneisses display strong LREE en-

richment, depleted HREE, and pronounced negative Eu anomalies, indicating plagioclase fractionation and crustal reworking processes typical of Archean continental crust evolution.

7) The granites are silica-rich, peraluminous, and show calc-alkaline to alkali-rich affinity. Trace element ratios, low K/Rb values, and pronounced negative Eu anomalies suggest derivation through partial melting of older continental crust combined with fractional crystallization, with limited mantle contribution.

8) The integrated field, petrographic, and geochemical evidence suggests that the Devanahalli region records a multi-stage Archaean crustal evolution involving early TTG crust formation, emplacement of mafic-ultramafic magmas, high-grade metamorphism, migmatization, and late-stage granitic intrusion.

9) Overall, the study area represents an important segment of the eastern Dharwar Craton and provides valuable insights into Archaean crust-forming processes, crustal reworking, and stabilization of the continental lithosphere in southern India.

10) The close spatial association between migmatitic gneisses and granitic intrusions, together with the occurrence of gneiss xenoliths within granites, indicates a strong petrogenetic relationship between the two lithologies.

11) The overlapping geochemical characteristics of gneisses and granites, including their peraluminous nature, enrichment of LREE over HREE, and consistent negative Eu anomalies, support a common crustal source and reflect significant involvement of feldspar during melting and differentiation processes.

12) The presence of migmatitic structures such as stromatic, ptygmatic, and schollen textures in the gneisses provides direct field evidence for partial melting of the crust, suggesting that the granitic magmas were most likely generated through anatexis of the older gneissic basement.

13) The integrated field, petrographic, and geochemical data collectively support a model of late Archaean crustal reworking in the Devanahalli area, where older TTG-type gneisses were partially melted during tectono-thermal events to produce younger granitic magmas.

14) Tectonic discrimination diagrams using Rb- (Y + Nb), Nb-Y, and Ta-Yb systematics (**Figures 43-45**) show that the granites consistently plot within the volcanic arc granite (VAG) to syn-collisional granite (Syn-COLG) fields.

15) The geochemical affinity indicated by these diagrams suggests that the granites were emplaced in a convergent margin tectonic setting, related to subduction and subsequent continental collision.

16) The depletion of high field strength elements (HFSE; Nb and Ta) and the relative enrichment of large ion lithophile elements (LILE) indicate a crustally derived magma source influenced by subduction-related processes.

17) Integration of tectonic discrimination results with field relationships and petrographic characteristics suggests that the granites were formed through partial melting of older continental crust.

18) These granitoids therefore represent products of Neoarchean crustal re-

working and stabilization, and record an important phase of the tectono-thermal evolution of the eastern Dharwar Craton.

Conflicts of Interest

The authors declare no conflicts of interest regarding the publication of this paper.

References

[1] Manikyamba, C. and Kerrich, R. (2012) Eastern Dharwar Craton, India: Continental Lithosphere Growth by Accretion of Diverse Plume and Arc Terranes. *Geoscience Frontiers*, **3**, 225-240. https://doi.org/10.1016/j.gsf.2011.11.009

[2] Martin, H., Smithies, R.H., Rapp, R., Moyen, J.-F. and Champion, D. (2005) An Overview of Adakite, Tonalite-Trondhjemite-Granodiorite (TTG), and Sanukitoid: Relationships and Some Implications for Crustal Evolution. *Lithos*, **79**, 1-24. https://doi.org/10.1016/j.lithos.2004.04.048

[3] Moyen, J. and Martin, H. (2012) Forty Years of TTG Research. *Lithos*, **148**, 312-336. https://doi.org/10.1016/j.lithos.2012.06.010

[4] Barbarin, B. (1999) A Review of the Relationships between Granitoid Types, Their Origins and Their Geodynamic Environments. *Lithos*, **46**, 605-626. https://doi.org/10.1016/s0024-4937(98)00085-1

[5] Frost, B.R., Barnes, C.G., Collins, W.J., Arculus, R.J., Ellis, D.J. and Frost, C.D. (2001) A Geochemical Classification for Granitic Rocks. *Journal of Petrology*, **42**, 2033-2048. https://doi.org/10.1093/petrology/42.11.2033

[6] Chadwick, B., Vasudev, V.N. and Hegde, G.V. (2000) The Dharwar Craton, Southern India, Interpreted as the Result of Late Archaean Oblique Convergence. *Precambrian Research*, **99**, 91-111. https://doi.org/10.1016/s0301-9268(99)00055-8

[7] Jayananda, M., Peucat, J., Chardon, D., Rao, B.K., Fanning, C.M. and Corfu, F. (2013) Neoarchean Greenstone Volcanism and Continental Growth, Dharwar Craton, Southern India: Constraints from SIMS U-pb Zircon Geochronology and Nd Isotopes. *Precambrian Research*, **227**, 55-76. https://doi.org/10.1016/j.precamres.2012.05.002

[8] Ramakrishnan, M. and Vaidyanadhan, R. (2010) Geology of India, Vol. 1. Geological Society of India.

[9] Singh, H.K., Kumar, Y., Chandrasekharam, D., Gurav, T. and Singh, B. (2014) High-heat-Producing Granites of East Dharwar Craton around Gugi, Karnataka, and Their Possible Influence on the Evolution of Rajapur Thermal Springs, Deccan Volcanic Province, India. *Geothermal Energy*, **2**, Article No. 2. https://doi.org/10.1186/s40517-014-0002-4

[10] Passchier, C.W. and Trouw, R.A.J. (2005) Microtectonics. Springer.

[11] Roy, S. and Mareschal, J. (2011) Constraints on the Deep Thermal Structure of the Dharwar Craton, India, from Heat Flow, Shear Wave Velocities, and Mantle Xenoliths. *Journal of Geophysical Research*, **116**, B02409. https://doi.org/10.1029/2010jb007796

[12] Mehnert, K.R. (1973) Migmatites and the Origin of Granitic Rocks. Elsevier.

[13] Rollinson, H. (1993) Using Geochemical Data: Evaluation, Presentation, Interpretation. Longman Scientific & Technical.

[14] O'Connor, J.T. (1965) A Classification for Quartz-Rich Igneous Rocks Based on Feldspar Ratios. U.S. Geological Survey Professional Paper, 525-B, B79-B84.

[15] Gill, R. (1981) Orogenic Andesites and Plate Tectonics. Springer-Verlag.

[16] Barker, F. and Arth, J.G. (1976) Generation of Trondhjemitic-Tonalitic Liquids and Archean Bimodal Trondhjemite-Basalt Suites. *Geology*, **4**, 596-600. https://doi.org/10.1130/0091-7613(1976)4<596:gotlaa>2.0.co;2

[17] Hunter, D.R., Brown, M. and Bickle, M.J. (1978) The Geochemistry of Archean Granitic Rocks. *Contributions to Mineralogy and Petrology*, **67**, 87-99.

[18] Pearce, J.A., Harris, N.B.W. and Tindle, A.G. (1984) Trace Element Discrimination Diagrams for the Tectonic Interpretation of Granitic Rocks. *Journal of Petrology*, **25**, 956-983. https://doi.org/10.1093/petrology/25.4.956

[19] Nutman, A.P., McGregor, V.R., Friend, C.R.L., Bennett, V.C. and Kinny, P.D. (1996) The Itsaq Gneiss Complex of Southern West Greenland; the World's Most Extensive Record of Early Crustal Evolution (3900-3600 Ma). *Precambrian Research*, **78**, 1-39. https://doi.org/10.1016/0301-9268(95)00066-6

[20] Chardon, D., Peucat, J., Jayananda, M., Choukroune, P. and Fanning, C.M. (2002) Archean Granite-Greenstone Tectonics at Kolar (South India): Interplay of Diapirism and Bulk Inhomogeneous Contraction during Juvenile Magmatic Accretion. *Tectonics*, **21**, 7-1-7-17. https://doi.org/10.1029/2001tc901032

[21] Taylor, S.R. and McLennan, S.M. (1985) The Continental Crust. Blackwell.

[22] Aadhiseshan, K.R. and Jayananda, M. (2025) Archean Crustal Evolution and Building of Habitable Continents: Insights from the Western Dharwar Craton. *Habitable Planet*, **1**, 197-220. https://doi.org/10.63335/j.hp.2025.0016